scientific reports

Check for updates

OPEN

Probabilistic modelling is superior to deterministic approaches in the human health risk assessment: an example from a tribal stretch in central India

Rajkumar Herojeet[1], Rakesh K. Dewangan[2], Pradeep K. Naik[2,3]✉ & Janak R. Verma[2]

This case drew national attention in 2018. About 100 people died and more than 300 hospitalized in a span of few years in a village of 1200 people in a tribal stretch in central India. Medical teams visiting the area reported severe renal failure and blamed the local eating and drinking habits as causative factors. This human health assessment based on geochemical investigations finds nitrate (NO_3^-) and fluoride (F^-) pollution as well in village's groundwater. Both deterministic and probabilistic techniques are employed to decipher the contamination pathways and extent of contamination. Source apportionments of NO_3^- and F^- and their relationship with other ions in groundwater are carried out through chemometric modelling. Latent factors controlling the hydrogeochemistry of groundwater too are explored. While hazard quotients (HQ) of the chemical parameters ($HQ_{NO_3^-}$ and HQ_{F^-}) identify ingestion as the prominent pathway, the calculated risk certainty levels (RCL) of the hazard index (HI) values above unity are compared between the deterministic and probabilistic approaches. Deterministic model overestimates the HI values and magnify the contamination problems. Probabilistic model gives realistic results that stand at infants ($HI_{NO_3^-} = 34.03\%$, $HI_{F^-} = 24.17\%$) > children ($HI_{NO_3^-} = 23.01\%$, $HI_{F^-} = 10.56\%$) > teens ($HI_{NO_3^-} = 13.17\%$, $HI_{F^-} = 2.00\%$) > adults ($HI_{NO_3^-} = 11.62\%$, $HI_{F^-} = 1.25\%$). Geochemically, about 90% of the samples are controlled by rock-water interaction with Ca^{2+}–Mg^{2+}–HCO_3^- (~ 56%) as the dominant hydrochemical facies. Chemometric modelling confirms Ca^{2+}, Mg^{2+}, HCO_3^-, F^-, and SO_4^{2-} to originate from geogenic sources, Cl^- and NO_3^- from anthropogenic inputs and Na^+ and K^+ from mixed factors. The area needs treated groundwater for human consumption.

Globally, consumption of nitrate (NO_3^-) and fluoride (F^-) contaminated groundwater is a serious concern due to their role in causing clinical diseases in humans[1–5]. Among the different inorganic forms of nitrogen (NO_3^-, NO_2^- and NH_4^+) that exist in aquifers, NO_3^- concentrations are higher than those of NO_2^- and NH_4^+ due to their high solubility and mobility rates as well as higher stable oxidative state in water[6,7]. Both NO_2^- and NH_4^+ are easily oxidized and converted to NO_3^-; thus, they have lower contents in groundwater[8]. Anthropogenic sources that contribute to excess NO_3^- in groundwater system are overuse of N-fertilizers, excreta from livestock farms, municipal wastewater irrigation, runoff from urban and agricultural land, leaching from waste dumping sites and discharge of untreated sewage and industrial effluents[9–13].

The natural sources of NO_3^- in groundwater are the dissolution and oxidation of nitrogenous minerals in the sedimentary and metasedimentary rocks. The bedrock nitrogen minerals, such as nitraline, nitre, suhalite and tobelite, have three possible origins: organic matter, ammonium silicates and nitrate and ammonium salts[14]. Dissolution of these sources release ammonium from their crystal lattices into the soil horizon, the chemical form which can be easily assimilated by soil micro-organisms or get converted to NO_3^- through the nitrification

[1]Department of Environmental Studies, Post Graduate Government College, Sector-11, Chandigarh 160011, India. [2]Central Ground Water Board, North Central Chhattisgarh Region, Ministry of Jal Shakti, Govt. of India, LK Corporates Tower, Dumartarai, Dhamtari Road, Raipur 492015, India. [3]Present address: Centre for Hydrological Sciences and Communication, Bhubaneswar, India. ✉email: pradeep.naik@water.net.in

process for nitrogen fixation by leguminous plants[15–17]. On the other hand, the weathering process of organic nitrogen present in bedrocks are mineralized and converted to ammonium, which is readily used by the soil biota.

Recently, many workers highlighted the worldwide contamination of NO_3^- in groundwater and its adverse effect on human health. Some locational examples are Loess Plateau, Northwest China[18], Weining Plain, North-west China[2], Matanza-Riachuelo River Basin, Argentina[19], Donsheng district, Inner Mongolia[20], Catalan Region, Spain[21], Gorveh-Dehgelan, Western Iran[22], Shanmuganadhi river basin, southern India[23], Jalandhar district, Punjab, India[24], Panipat district, Haryana, India[25], Nagpur, Western Maharashtra, India[26], Gaya district, Bihar, India[8], Tiruppur, Tamil Nadu, India[27].

Water with NO_3^- concentrations between 45 and 100 mg/L and above 100 mg/L are consumed daily for drinking purposes by ~ 118 million and ~ 108 million people, respectively, in India[28,29]. The common and predominant effect of excess NO_3^- content (> 45 mg/L) in bottle-fed infants and children is Methemoglobinemia disease[24,30]. Almasri concludes that the clinical symptom of methemoglobinemia is normally encountered as body dehydration and gastrointestinal infections[31]. Further, the biochemical effects of NO_3^- occur in the human body as follows: (a) NO_3^- is converted to NO_2^- under reducing conditions, (b) haemoglobin (Hb) combines with NO_2^- to form methemoglobin, (c) the effect of methemoglobin reduces the oxygen supply in red blood cells and drops the oxygen level in the body and (d) higher rate of methemoglobin formations ($> 10\%$) leads to the blueish colouration of the skin, known as a blue-baby syndrome (cyanosis)[4,32]. The prolonged exposure to high NO_3^- content in water has other health risks, such as multiple sclerosis, nitrosamines and non-hodgkin lymphoma[33–35].

The fluoride deposition on the earth's crust is approximately 0.32% and occurs mainly in rocks, such as granites and gneisses. Both natural and anthropogenic inputs contribute to F^- contamination in groundwater. However, the higher concentrations of F^- in groundwater is predominantly from geogenic sources and their exposure is a threat to human health[36]. The geogenic sources include presence of fluoride-bearing minerals, such as fluorite, amphiboles, topaz, apatite, fluorapatite, etc. in rocks, sediments and soils, evapotranspiration and atmospheric deposition[37–39]. Prominent anthropogenic sources are the applications of pesticides and phosphatic fertilizers, industrial effluents and landfills[40–42].

Lower F^- concentrations (< 0.5 mg/L) in drinking water cause dental carries and concentrations between 0.6 and 1.5 mg/L are essential for bone formation and development of skeleton and teeth in the human body[4,24,43]. The long-term exposure to F^- concentrations above the recommended guideline/permissible limit (1.5 mg/L) may cause dental fluorosis, discoloration, pitting and mottling of teeth, skeleton fluorosis (4–8 mg/L), osteoporosis, arthritis, thyroid, rheumatic pain, kidney problem, muscle stiffness and abnormalities in red blood cells (> 10 mg/L)[38,44–47]. Globally, at least 200 million individuals are affected by acute fluorosis in 28 different nations due to the consumption of F^- contaminated groundwater[48]. In India alone, ~ 25 million individuals are affected by endemic fluorosis in 20 states besides ~ 66 million people in the risk of developing fluorosis, including ~ 6 million children below 14 years of age[49–52]. Mukherjee and Singh have made a detailed review of F^- contamination in groundwater in different states of India[53].

Supebeda, the study area of this contribution, is a small village situated in the border of Chhattisgarh and Odisha States in a tribal stretch in central India (Fig. 1). Groundwater is the primary source of water in this region. In recent years, the local inhabitants have been facing numerous medical problems related to severe renal issues, kidney diseases and fluorosis. As per the media reports, there have been more than 100 causalities till date due to these diseases in recent years and around 300 villagers are battling for life. Thus, the study area has become a hotspot to understand the real reason for the peoples' health problems. Several research organizations, such as the Indian Council of Medical Research, Geological Survey of India, Indira Gandhi Agricultural University, Chhattisgarh State Public Health and Engineering Department, Pandit Ravishankar Shukla University, National Institute Technology (Raipur), have already visited the village for investigation purposes. The research angles by many of these organizations have been genetic genesis, food habits, consumption of spurious liquor and other medicinal causes[54–56]. Presently, there is no literature available on the geochemistry of groundwater quality and associated health hazard risks to the local population. Preliminary sampling suggested NO_3^- and F^- contamination in groundwater[57]. The present investigation, therefore, is aimed at making a detailed appraisal of the groundwater quality, non-carcinogenic health risk assessment in humans based on deterministic and probabilistic approaches, hydrochemical characterization, source apportionment of NO_3^- and F^- through chemometric techniques and their relationship with other ions in groundwater.

Materials and methods
Study area
The study area, village Supebeda, lies between North latitudes 19° 50′ and 19° 54′ and East longitudes 82° 38′ and 82° 42′ occupying a geographical area of 3 km² in the administrative block of Deobhog in Gariyaband district of Chhattisgarh State, India (Fig. 1). Situated on the bank of the river Tel, it borders the State of Odisha in the east. With a population of about 1200 people, it has nearly equal male–female sex ratio and literacy rate of 50.51%. The village has a Gram Panchayat (village council). The region is endowed with a sub-tropical monsoon climate with three distinct seasons: the southwest monsoon starts from mid-June to September; the winter season spreads from October to February and the summer season extends from March to mid-June. The average annual rainfall is 1200 mm, and the temperature in winter varies from 5 to 25 °C and in summer from 29 °C to 46 °C.

Local geology
Gupta et al.[58] and Neogi and Das[59] have conducted detailed study on the geology of the area. As per this study, there are three major lithological units in the area from east to west, i.e., (i) migmatiticquartzo feldspathic gneiss, (ii) banded augen gneiss and (iii) hornblende granite (Fig. 2). Migmatiticquartzo feldspathic gneisses are grey-colored, medium-grained rocks with finely laminated alternations of felsic (quartz + plagioclase + K-feldspar:
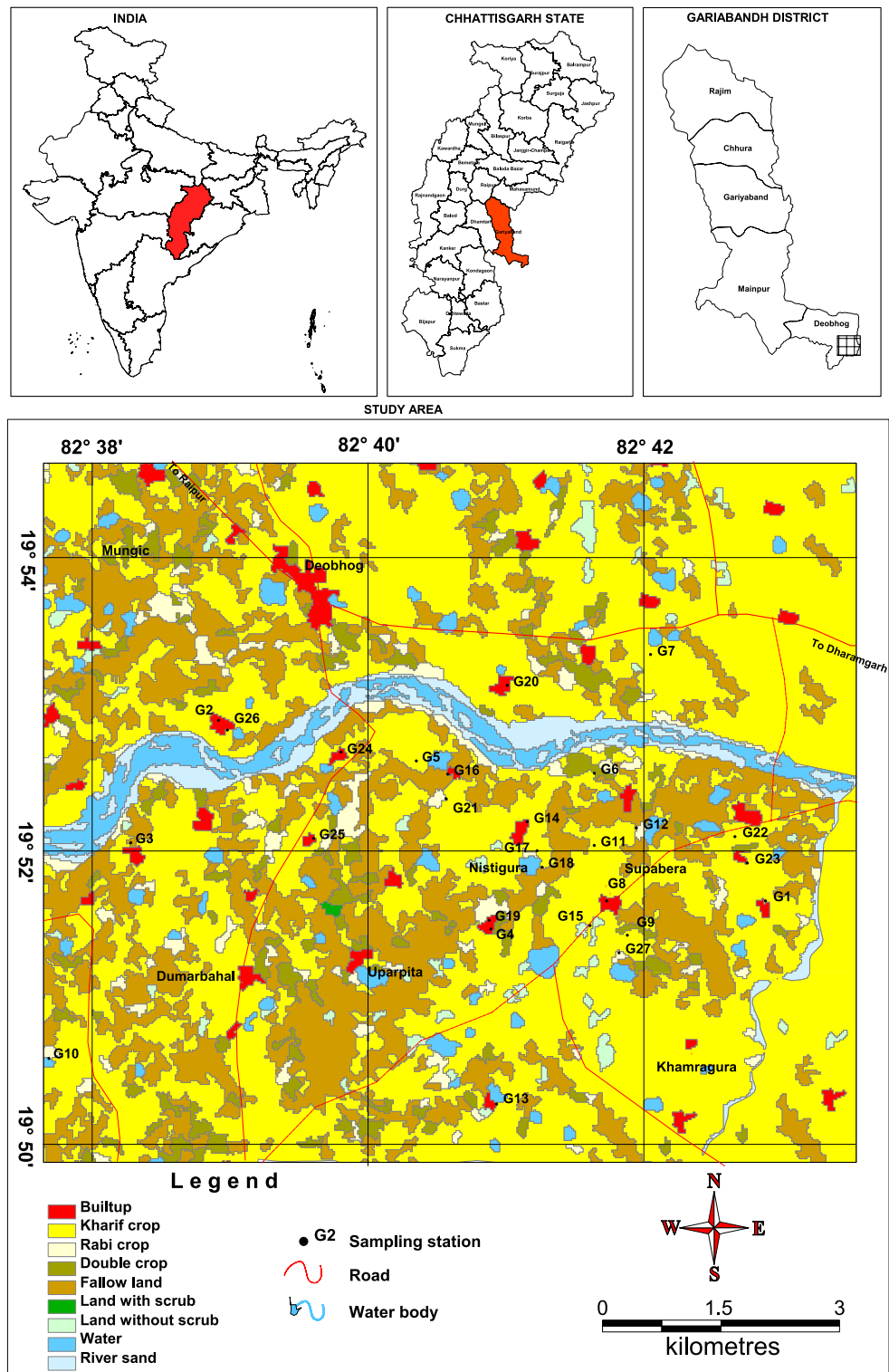
Figure 1. Groundwater sampling around village Supebeda in Chhattisgarh State, India: The village borders the state of Odisha on its east. Groundwater samples were collected from 27 locations marked by black dots. The map was prepared based on MapInfo 8.5 (https://www.precisely.com/product/precisely-mapinfo/mapinfo-pro).

Qtz + Pl + Kfs) and mafic (Bt + Hbl-rich) bands. Leucocratic segregations are found extensively and are generally stromatically folded into or parallel to the layering. There is occasional presence of orthopyroxenes in migmatite gneisses as greasy, green patches with diffuse margins ('patchy charnockite'). Bands of migmatized mafic
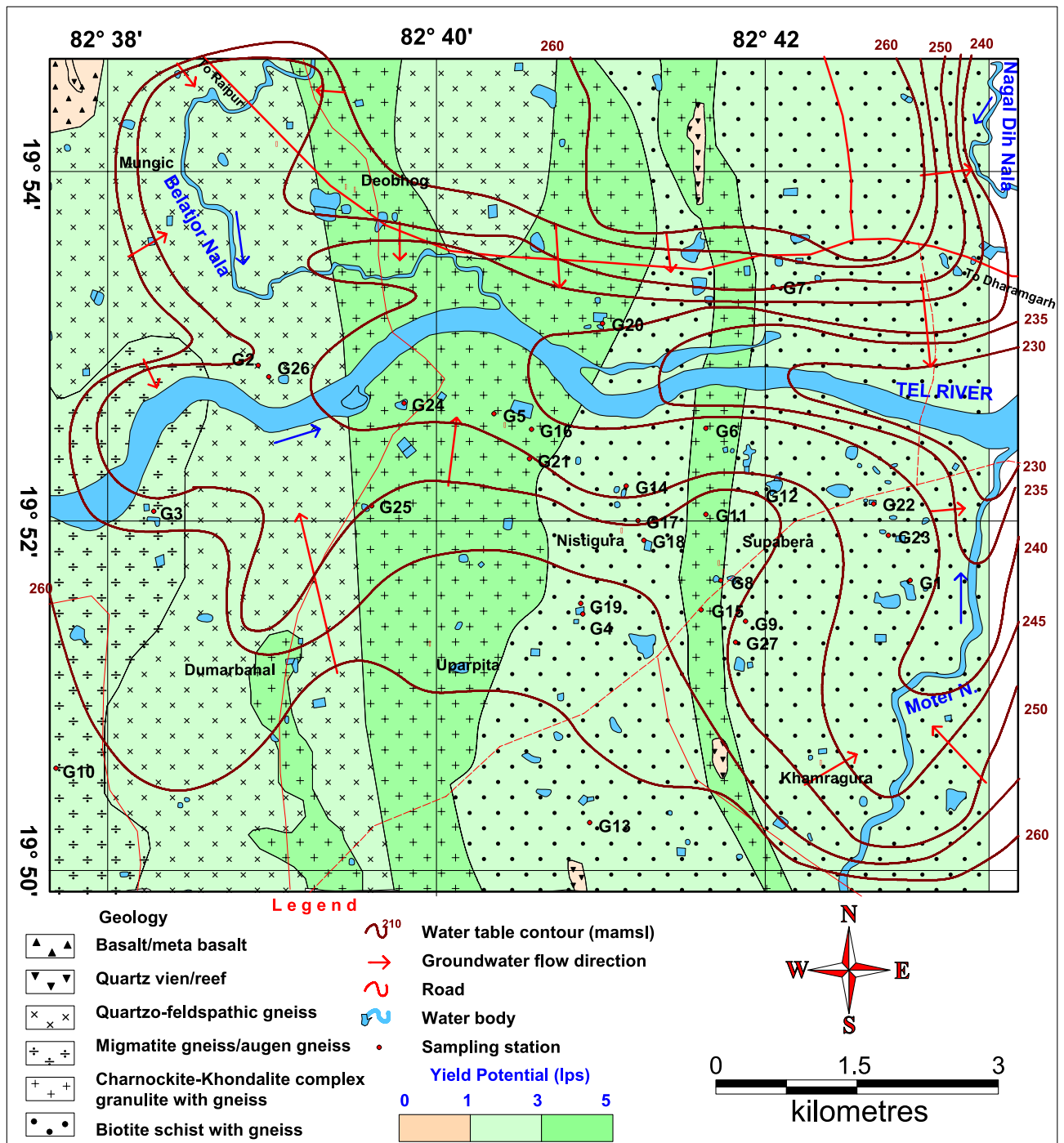
Figure 2. Geology and hydrogeology of the area around village Supebeda in Chhattisgarh State, India: The area represents a metamorphic terrain with a complex geology[58]. The arrow marks show the groundwater flow in different directions. Well drilled in the charnokite-khondalite complex are high-yielding with a yield potential of 3–5 L per second. The map was prepared based on MapInfo 8.5 (https://www.precisely.com/product/precisely-mapinfo/mapinfo-pro).

granulites, metapelitic rocks (infrequently sapphirine-bearing) and rare calcsilicate granulites, besides isolated appearance blastoporphyritic charnockite, occur congruently with the gneisses.

Banded augen gneisses are pink-colored, medium- to coarse-grained rocks. The bandings within them are defined by mafic and felsic layers with K-feldspar (Kfs) augen and quartz lenticles. There is occasional occurrence of leucosomes in a narrow zone closer to the migmatitic quartzofeldspathic gneiss unit with sharp abetment to the west. The gneissic fabric generally precedes the leucosomes in banded augen gneiss. Hbl-rich and Pl + Cpx-rich layers are hosted thinly within banded gneisses. Amphibolites (Hbl + Pl ± Grt ± Cpx) and calc-silicate gneisses with these thin layers are mesoscopic to the regional scale bands.

Intruding into the banded gneiss is the pink-colored, coarse-grained hornblende granite that consists of microcline, quartz, hornblende, and biotite. With intense shearing and mylonitization along its eastern fringe, it has poor presence further westward.

Hydrogeology

Groundwater occurs under unconfined condition in weathered portions of rocks and semi-confined to confined conditions in their fractured parts, i.e., in charnockite and khondalite, at depth. The shallow aquifer occurs within an average depth of 16 m. The configuration of water table in the shallow aquifer follows the topography due to which the groundwater movement is generally toward valleys or topographic lows. The water bodies, such as tanks, canals, and streams. also influence the occurrence and movement of groundwater in shallow aquifer. This aquifer is developed mostly by dugwells in the area with their depth ranging between 7 and 16 m. In general, the yield of dugwells ranges from 25 to 40 m^3/day. Deeper aquifer in the area is formed mainly of granitic rocks and is developed by borewells with a depth range of 50–80 m. In general, the yield of borewells ranges from 85 to 430 m^3/day.

The groundwater flow is analyzed based on the water table elevation contours. In northern part of the study area, groundwater flow is toward the south, i.e., the Tel River, while the flow is toward the north in the southern part. The water table elevations in the study area range between 240 and 260 m above mean sea level with northern part having higher groundwater table elevation. Transmissivity ranges from 15 to 45 m^2/day in charnockite and khondalite and at favourable places it goes up to 100 m^2/day. The potential fractures for boreholes up to 80 m depth are recorded at various depths, i.e., 40–45, 60–65, 75–80 m, and are 3–4 in numbers. Hydrogeology of the study area is shown in Fig. 2.

Water sampling and analysis

Groundwater samples from twenty-seven locations were collected from the dugwells and borewells in and around the Supebeda area during pre-monsoon season (May 2020) (Fig. 1). Plastic bottles (HDPE) of 1000 ml capacity were used. These bottles were prewashed with HNO_3 (10%) and rinsed with double deionised water. At the time of sample collection, groundwater sources were flushed for 10–15 min to obtain a fresh solution by removing the stagnant water in the pipe. The sampling bottles were thoroughly rinsed 2–3 times with the fresh groundwater to be collected to preserve the original characteristics of the sampled water. Some basic parameters, such as pH, electrical conductivity (EC) and total dissolved solids (TDS), were immediately measured onsite after the collection of groundwater samples using a pH/EC/TDS meter (Hanna HI 9811-5). Whatman filter paper (0.45 μm) was used to remove the suspended particulate matter. The samples were preserved by acidifying (pH ~ 2 with HNO_3) and kept at a temperature of 4 °C. Standard protocol prescribed by the American Public Health Association was followed for the investigation of major cations (Ca^{2+}, Mg^{2+}, Na^+, and K^+) and anions (HCO_3^-, Cl^-, SO_4^{2-}, F^-, and NO_3^-). Merck-GR grade chemicals and reagents were used to prepare the chemical solutions using double deionized water. All the glassware and apparatus were soaked with 10% hydrochloric acid (HCl) for one day and cleaned with double deionized water. Blank samples were prepared from the stock solutions of each parameter for instrumental calibration. The accuracy of analysing datasets was computed using the charge balance error (CBE) equation (Eq. 1), and each sample value was within its error limit of ± 5%[60].

$$\text{CBE\%} = \frac{\sum (Cations)meq/L - \sum (Anions)meq/L}{\sum (Cations)meq/L + \sum (Anions)meq/L} \times 100 \qquad (1)$$

Human health risk assessment (HHRA)

Human health risk assessment (HHRA) is the quantitative risk analysis of potentially harmful chemical parameters present in water on human health through various pathways and specific time periods[61,62]. It has four distinct steps: (1) hazard identification, (2) exposure assessment, (3) dose–response assessment and (4) risk characterization[4,63].

The significant pathways for risk analysis on human health from chemical exposure are ingestion and dermal contact. In the present study, the average daily dose (ADD) of ingestion and dermal pathways for target chemicals, namely NO_3^- and F^-, are employed to determine the non-carcinogenic HHRA as shown in Eqs. (2) and (3)[64]. The assessments of $ADD_{ingestion}$ and ADD_{dermal} are computed on four different age groups, i.e., infants (< 1 year), children (1–11 years), teens (11–18 years) and adults (above 18 years). The adverse impact of the target parameters on human health may vary due to physiological and behavioural attributes, organ development factors and tolerance responses to the specific chemicals in the human body.

$$ADD_{ingestion} = \frac{C_M \times IR_w \times EF_r \times ED}{BW \times AT_r} \qquad (2)$$

$$ADD_{dermal} = \frac{C_M \times SA \times K_p \times EF_r \times ED \times ET \times CF}{BW \times AT_r} \qquad (3)$$

(The parameters/variables used in these equations are defined in Supplementary Table S1).

The ratio of the potential adverse non-carcinogenic risk from each exposure pathway (ingestion and dermal) with respect to the corresponding reference dose of a chemical parameter is estimated through hazard quotient (HQ)[64], as shown in Eqs. (4)–(5). Hazard index (HI) is the combined non-carcinogenic hazard risks of a particular parameter from all different possible exposure routes[65,66]. Both HI and HQ are unitless values. When HQ > 1, it

is indicative of potential health effects from a specific exposure route[67]. Similarly, the value of $HI > 1$ depicts the adverse non-carcinogenic toxicity in each target age group[67].

$$HQ_{ingestion} = \frac{ADD_{ingestion}}{RfD_i} \tag{4}$$

$$HQ_{dermal} = \frac{ADD_{dermal}}{RfD_d} \tag{5}$$

$$HI_M = \sum_{i=1}^{n} HQ_{ingestion} + \sum_{i=1}^{n} HQ_{dermal} \tag{6}$$

where HI_M indicates the total hazard index of a specific parameter, and i represents the exposure route of a specific subpopulation group considered in the present study (Eq. 6). The ingestion and dermal pathways reference dose (RfD) values for NO_3^- and F^- are 1.6 mg/kg per day and 0.06 mg/kg per day, respectively[4,68–70].

Both deterministic and probabilistic approaches are applied to determine the potential non-carcinogenic HHRA in the present study. The deterministic approach simply incorporates fixed values on the mathematical formula developed by USEPA for different exposure pathways[71]. The point estimation results generate only a single value that may underestimate or overestimate the risk analysis. Normally, the values of the variables of the point estimation vary with respect to climatic conditions, place, time, chemical concentrations in water and receptor types (i.e., body weight, exposure frequency and different subpopulation groups)[72], but since the uncertainty of the deterministic model considers only a fixed value for every input variable, this technique is a conservative risk assessment approach.

Probabilistic technique, namely Monte Carlo Simulation (MCS), is an alternative statistical model that offers a sound methodology and provides holistic information for risk assessment suggested by USEPA[72]. Monte Carlo Simulation is a computer software application configuring a statistical distribution array in the form of probabilistic approximation of a mathematical equation to generate more corroborated reproducibility results and reduces the uncertainty associated in risk analysis[4]. Oracle Crystal Ball software version (11.1.2.4.850) is used for the MCS study. The operation of MCS requires prearrangement of input variables/parameters with respect to their maximum, minimum, mean, and standard deviation (SD) values to define best-fitted statistical distribution types to generate their probability distribution functions (PDFs)[72]. The input parameters, such as ingestion rate (IR_w), exposure frequency (EF), exposure duration (ED), expose skin surface area (SA), exposure time (ET) and body weight (BW), generally have 10,000 repetitions for the computation of risks from oral ingestion and dermal contact for each subpopulation group. Thus, the numerical stability of MCS is obtained at 10,000 permutations for HQ and HI[4,73,74]. The sensitivity analysis is also employed to extract the significant input variables impacting the outcome of a simulation model for potential risks.

In this work, the target parameters, i.e., NO_3^- and F^-, are defined by the auto-select to determine the best-fitted probability distribution pattern based on their concentration values. Their goodness of fit (GoF) statistical outcomes are presented in Table 1. The values and types of distribution of various input variables for ingestion and dermal pathways for the deterministic and probabilistic models are provided in Supplementary Table S1.

Chemometric analysis

Chemometric statistical models, such as principal component analysis (PCA) and cluster analysis (CA), are widely used by many researchers to distinguish among the probable sources of chemical parameters in water[11,75–78]. Principal component analysis enables extraction of valuable information and better interpretation of statistically significant parameters from large, complex datasets[79]. The present study uses z-scale standardization of all chemical parameters to generate dimensionless values[80–82]. Varimax rotation method has been employed to extract the principal components (PCs). The PCs with eigenvalues > 1 are statistically significant for interpreting the hidden factors in water quality[83,84].

Cluster analysis has been used to create similar groups from a different set of objects or variables[85]. Ward's linkage and squared Euclidean distance have been applied on z-transformation data to obtain different clusters[86]. The cluster significance has been assessed using Sneath's test method[87]. Minitab 17 and MS Office 2021 have been employed to perform the statistical analysis.

Parameters	Distribution types and their parameter values	Anderson–Darling test	Anderson–Darling test (p value)	Kolmogorov–Smirnov test	Kolmogorov–Smirnov test (p value)	Chi-square test	Chi-square test (p value)
Premonsoon							
Nitrate	Logistic (Mean = 34.25, Scale = 24.04)	14,593	0.000	0.1940	0.000	14.667	0.001
Fluoride	Uniform (Min = 0.01, Max = 1.97)	0.5670	0.543	0.1815	0.250	5.0370	0.081

Table 1. Best fitted and goodness of fit (GoF) outcomes of the probability distribution of Nitrate and Fluoride in the groundwater around village Supebeda in Chhattisgarh State, India.

Results and discussions

Table S2 lists the concentrations of various physicochemical parameters in analyzed groundwater samples. Table 2 gives the statistical description of physicochemical parameters [range, mean, and standard deviation (SD)] and percentage of samples above the BIS[46] and WHO[45] standards. Water samples are neutral to slightly alkaline in nature with the pH values ranging from 7.2 to 8.3 with a mean of 7.9 (mean ± SD = 7.9 ± 0.3). EC values show wide variation from 313.0 to 3446.0 μS/cm with 11.11% samples above the guideline value of 1500 μS/cm[45]. High EC values at some locations cause salinity due to excessive mineralization in groundwater. The water quality classification based on EC values[88] indicates that 62.96% of the samples are moderately saline, 26.63% are medium to highly saline and 7.41% are highly saline for irrigation purposes (Table S3). Further, classification by FAO[89] shows that 7.41% samples are above the standard EC range (0–3000μS/cm) for irrigational use (Table 2).

Groundwater samples with TDS values above acceptable limit of 500 mg/L and permissible limit of 2000 mg/L[46] for drinking purposes are 22.22% and 11.11%, respectively, of all collected samples. These 11.11% of the samples are above the normal range of 0–2000 mg/L[89] for irrigational use as well. As per Davis and DeWiest[90], about 63% of the samples are within the desirable limit for drinking purposes and about 26% in between desirable and permissible limit of 1000 mg/L (Table S3). Further, the TDS classification by Freeze and Cherry[91] indicates that majority of the groundwater samples (88.89%) falls under freshwater and the rest 11.11% under brackish water category (Table S3).

Total hardness (TH) values vary from 65.0 to 755.0 mg/L with 33.33% and 11.11% samples above the acceptable (200 mg/L) and permissible limits (600 mg/L), respectively[46]. The elevated level of TH is primarily linked with the excess concentrations of Ca^{2+}, Mg^{2+} and HCO_3^- ions in groundwater[11,76]. Classification of groundwater based on TH values by Sawyer and McCarty[92] divulges that 3.70% of the samples are soft, 22.22% are moderately hard, 44.44% are hard and 29.63% are very hard in nature (Table S3). Further, TDS versus TH plot depicts that the groundwater is fresh to brackish water types with moderately hard to very hard in nature (Fig. S1). Sindhu concludes that the prolonged consumption of very hard water is associated with calcification of arteries, urolithiasis, anencephaly, and gastrointestinal tract irritation[93]. Box-Whisker plot shows the relative abundance and dominance of various cations ($Ca^{2+} > Na^+ > Mg^{2+} > K^+$) and anions ($HCO_3^- > Cl^- > NO_3^- > SO_4^{2-} > F^-$) in groundwater (Fig. S2).

Major parameters

About 26.9% and 3.7% samples show Ca^{2+} contents above the acceptable limit of 75 mg/L and permissible limit of 200 mg/L, respectively[46]. The Mg^{2+} mean ± SD is 21 ± 13.2 with 11.11% of samples above the acceptable limit of 30 mg/L[46] (Table 2). The alkali metals, i.e., Na^+ and K^+, are within their respective guideline values (200 mg/L and 12 mg/L)[45]. HCO_3^- concentrations range from 85 to 519 mg/L with 3.7% of samples above the guideline value of 500 mg/L[45]. Chloride (Cl^-) concentrations vary from 7.1 to 408.3 mg/L, with 11.11% of samples above the acceptable limit of 250 mg/L[46]. The excess concentrations of Ca^{2+}, Mg^{2+}, HCO_3^- and Cl^- ions are the key chemicals resulting hardness of groundwater[24]. The level of SO_4^{2-} ions in groundwater is within the acceptable limit of 200 mg/L[46]. The concentrations of cations (Ca^{2+}, Mg^{2+}, and Na^+) and anions (HCO_3^-, Cl^-, and SO_4^{2-}) are within their normal ranges for irrigational use (Table 2)[89].

Parameter	BIS[46] standards		FAO[89]	Premonsoon		% of sample above BIS[46] and WHO[45] Standards		
	AL	PL	Standards (usual range for irrigation use)	Range	Mean ± SD	AL	PL	% of sample above FAO[89] Standards
Physical parameters								
pH	6.5–8.5		6.5–8.4	7.2–8.3	7.9 ± 0.3	NIL		NIL
EC	1500[a]		0–3000	313.0–3446.0	941 ± 795	11.11% (3)		7.4% (2)
TDS	500	2000	0–2000	200.32–2205.44	602.2 ± 509.0	22.22% (6)	11.11% (3)	11.11% (3)
TH	200	600	–	65.0–755.0	257 ± 178	33.33% (9)	11.11% (3)	–
Major cations								
Ca^{2+}	75	200	0–400	20.0–214.0	67 ± 53	29.6% (8)	3.7% (1)	NIL
Mg^{2+}	30	100	0–60	3.6–52.8	21 ± 13.2	11.11% (3)	NIL	NIL
Na^+	200[a]		0–920	16.4–185.5	65 ± 43.9	NIL		NIL
K^+	12[a]		–	0.6–11.4	2.2 ± 2.1	NIL		–
Major anions								
HCO_3^-	500[a]		0–610	85.0–519.0	297 ± 109	3.7% (1)		NIL
Cl^-	250	1000	0–1063	7.1–408.3	73.8 ± 109.2	11.11% (3)	NIL	NIL
SO_4^{2-}	200	400	0–960	4.8–105.5	29 ± 30.6	NIL	NIL	NIL
NO_3^-	45		0–45	0–128.3	39 ± 40	37.0% (10)		37.0% (10)
F^-	1	1.5	0–20	0–1.9	0.9 ± 0.6	14.8% (4)	25.9% (7)	NIL

Table 2. Descriptive statistics of chemical parameters of groundwater samples collected from Supebeda, district Gariyaband, Chhattisgarh, India. AL and PL stands for acceptable limits and permissible limits in the absence of alternative source of water (BIS[46]). [a]Indicates parameters guideline values as per WHO[45].

Health risk parameters

Consumption of NO_3^- and F^--rich water causes various health risks in humans. The NO_3^- content in groundwater in Supebeda exceeds its guideline value of 45 mg/L for drinking and irrigation purposes[46,89] in 37.0% of samples (Table 2). The classification of NO_3^- concentrations based on Adimalla[43] signifies that 62.96% of the samples have no risk (< 45 mg/L), 29.63% of samples have high risk (45–100 mg/L) and the remaining 7.41% of samples have very high risk to human health (> 100 mg/L) (Table S4).

The range of F^- concentrations varies from 0 to 1.9 mg/L with 14.8% and 25.9% of samples above the acceptable limit of 1.0 mg/L and permissible limit of 1.5 mg/L, respectively[46]. Although about 55.56% of samples have the required F^- level (0.6–1.5 mg/L) for human health, as per Adimalla[43], 22.22% of samples may cause dental caries (< 0.5 mg/L) and an equal percent dental fluorosis (1.6–2.0 mg/L) (Table S4).

Health risk assessment (HRA)

Table S5 provides the calculated average daily dose (ADD) values of NO_3^- and F^- through ingestion and dermal contact of groundwater using deterministic and probabilistic approaches for different age groups. Tables 3 and 4 show estimates of the non-carcinogenic HRA with respect to hazard quotient (HQ) and hazard index (HI) parameters, respectively. The deterministically calculated mean, median, 5th percentile (minimum) and 95th percentile (maximum) values of $HQ_{ingestion}$, HQ_{dermal} and HI for NO_3^- and F^- are relatively more than those of the probabilistically estimated values in all target population groups. The mean and 95th percentile of $HQ_{NO_3^-}$ for ingestion pathway are above the acceptable limit (i.e., HQ > 1) in the deterministic study, which indicates that the potential non-carcinogenic risk shall affect the larger sections in all target populations. On the other hand, the probabilistically calculated $HQ_{NO_3^-}$ for ingestion pathway is above the threshold limit (i.e., HQ > 1) only at 95th percentile, which shows that the clinical risk of non-carcinogenic effect is a concern to the sensitive sections of people in all subpopulation groups at the extreme point (Table 3).

In deterministic estimate, the ingestion route of HQ_{F^-} shows mean and 95th percentile above the safety limit (HQ > 1) only in infants, and rest of the population groups (Children, Teens, and Adults) have $HQ_{F^-} > 1$ in 95th percentile. In probabilistic study, the threat of non-carcinogenic hazard divulges at the maximum point (HQ_{F^-} 95th percentile > 1) through ingestion pathway in the infants and children's groups (Table 3). In dermal contact, the deterministically and probabilistically calculated mean, median, 5th percentile and 95th percentile values $HQ_{NO_3^-}$ and HQ_{F^-} are less than the threshold limit (HQ < 1) in all target population groups. This indicates that there is no potential non-carcinogenic health risk through dermal contact from the indicator parameters (Table 3).

Risk certainty level (RCL) is assessed to generate the likelihood percentage scenarios of non-cancer hazard quotient risk above the threshold value (HQ > 1) in all individual datasets of a particular pathway. It is always advantageous to determine the RCL value in HRA for any exposure pathway, even if the mean, 5th percentile and 95th percentile values of different age groups are below their threshold limits. Among the target age groups, the order of deterministic RCL (HQ > 1) for NO_3^- and F^- through the ingestion route is infants ($HQ_{NO_3^-}$ = 51.85% and HQ_{F^-} = 66.67%) > children ($HQ_{NO_3^-}$ 48.15% and HQ_{F^-} = 33.33%) > adults ($HQ_{NO_3^-}$ = 40.74% and

Premonsoon		Deterministic value (ingestion)					Risk certainty level (RCL) %	Probabilistic value (ingestion)					Risk certainty level (RCL) %
Age group	Parameter	Mean	Median	SD	5th percentile	95th percentile	HQ > 1	Mean	Median	SD	5th percentile	95th percentile	HQ > 1
Infants	$HQ_{NO_3^-}$	2.20E+00	1.22E+00	2.26E+00	1.69E−02	5.88E+00	51.85%	9.04E−01	5.27E−01	2.49E+00	−7.45E−01	3.74E+00	34.02%
Children		1.43E+00	7.90E−01	1.46E+00	1.10E−02	3.81E+00	48.15%	5.47E−01	3.52E−01	1.45E+00	−5.54E−01	2.24E+00	23.00%
Teens		1.03E+00	5.70E−01	1.06E+00	7.91E−03	2.75E+00	37.04%	3.84E−01	2.51E−01	1.01E+01	−3.92E−01	1.54E+00	13.16%
Adults		1.11E+00	6.13E−01	1.14E+00	8.52E−03	2.96E+00	40.74%	3.25E−01	2.43E−01	9.26E−01	−3.72E−01	1.45E+00	11.62%
Infants	HQ_{F^-}	1.41E+00	1.05E+00	8.84E−01	3.01E−01	2.82E+00	66.67%	7.32E−01	4.92E−01	1.54E+00	4.16E−02	2.23E+00	24.17%
Children		9.14E−01	6.83E−01	5.73E−01	1.95E−01	1.82E+00	33.33%	4.68E−01	3.53E−01	8.95E−01	3.12E−02	1.30E+00	10.55%
Teens		6.59E−01	4.92E−01	4.13E−01	1.41E−01	1.31E+00	25.93%	2.86E−01	2.03E−01	5.53E−01	9.03E−03	8.36E−01	2.00%
Adults		7.09E−01	5.30E−01	4.44E−01	1.51E−01	1.42E+00	33.33%	2.76E−01	2.02E−01	5.27E−01	9.08E−03	7.85E−01	1.25%
	Parameter	Deterministic value (dermal)					HQ > 1	Probabilistic value (dermal)					HQ > 1
Infants	$HQ_{NO_3^-}$	6.65E−03	3.68E−03	6.81E−03	5.11E−05	1.77E−02	NIL	4.09E−04	2.63E−04	1.06E−03	−3.64E−04	1.63E−03	NIL
Children		4.99E−03	2.76E−03	5.11E−03	3.83E−05	1.33E−02	NIL	4.54E−04	2.94E−04	1.19E−03	−3.96E−04	1.77E−03	NIL
Teens		4.73E−03	2.62E−03	4.85E−03	3.64E−05	1.26E−02	NIL	3.54E−04	2.38E−04	9.20E−04	−3.22E−04	1.40E−03	NIL
Adults		5.71E−03	3.16E−03	5.85E−03	4.39E−05	1.52E−02	NIL	3.16E−04	2.13E−04	8.22E−04	−3.21E−04	1.26E−03	NIL
Infants	HQ_{F^-}	4.25E−03	3.18E−03	2.66E−03	9.08E−04	8.89E−03	NIL	3.30E−04	2.46E−04	6.34E−04	2.38E−05	9.15E−04	NIL
Children		3.19E−03	2.38E−03	2.00E−03	6.81E−04	6.37E−03	NIL	3.63E−04	2.66E−04	7.04E−04	2.42E−05	1.02E−03	NIL
Teens		3.03E−03	2.26E−03	1.90E−03	6.46E−04	6.04E−03	NIL	2.64E−04	1.94E−04	5.03E−04	9.71E−06	7.51E−04	NIL
Adults		3.65E−03	2.73E−03	2.29E−03	7.80E−04	7.29E−03	NIL	2.41E−04	1.79E−04	4.62E−04	7.47E−06	6.87E−04	NIL

Table 3. Statistical description of deterministically and probabilistically calculated hazard quotient (HQ) for ingestion and dermal pathways in different age groups.

Age group	Pathways (ingestion + dermal)	Deterministic value					Risk certainty level (RCL) (%)	Probabilistic value					Risk certainty level (RCL) (%)
		Mean	Median	SD	5th percentile	95th percentile	$HI > 1$	Mean	Median	SD	5th percentile	95th percentile	$HI > 1$
Infants	$HI_{NO_3^-}$	2.21E+00	1.22E+00	2.27E+00	1.70E-02	5.90E+00	51.85%	9.05E-01	5.27E-01	2.49E+00	−7.45E-01	3.74E+00	34.03
Children		1.43E+00	7.93E+00	1.47E+00	1.10E-02	3.83E+00	48.15%	5.48E-01	3.35E-01	1.45E+00	−5.55E-01	2.24E+00	23.01
Teens		1.03E+00	5.72E-01	1.06E+00	7.95E-03	2.76E+00	40.74%	3.84E-01	2.51E-01	1.02E+00	−3.92E01	1.54E+00	13.17
Adults		1.11E+00	6.16E-01	1.14E+00	8.56E-03	2.97E+00	40.74%	3.52E-01	2.43E-01	9.26E-01	−3.72E-01	1.45E+00	11.62
Infants	HI_{F^-}	1.41E+00	1.06E+00	8.87E-01	3.02E-01	2.82E+00	66.67%	7.32E-01	4.92E-01	1.54E+00	4.18E-02	2.23E+00	24.17
Children		9.17E-01	6.85E-01	5.75E-01	1.96E-01	1.83E+00	37.04%	4.68E-01	3.53E-01	8.95E-01	3.15E-02	1.30E+00	10.56
Teens		6.62E-01	4.94E-01	4.15E-01	1.41E-01	1.32E+00	25.23%	2.86E-01	2,04E-01	5.53E-01	9.34E-03	8.36E-01	2.00
Adults		7.13E-01	5.33E-01	4.47E-01	1.52E-01	1.42E+00	33.33%	2.76E-01	2.02E-01	5.27E-01	9.34E-03	7.85E-01	1.25

Table 4. Statistical description of deterministically and probabilistically calculated hazard index (*HI*) for ingestion and dermal pathways in different age groups.

$HQ_{F^-} = 33.33\%$) > teens ($HQ_{NO_3^-} = 37.04\%$ and $HQ_{F^-} = 25.93\%$) (Table 3). Similar findings of NO_3^- and F^- non-carcinogenic health risk for groundwater ingestion pathways are found in Jiangcungou, Northwest China (i.e., children > adults > teenagers)[1] and Nalagarh valley, Himachal Pradesh, India (i.e., infants > children > adults > teenagers)[4]. On the other hand, the probabilistic *RCL* (*HQ* > 1) orders for NO_3^- and F^- through ingestion pathway are infants ($HQ_{NO_3^-} = 34.02\%$ and $HQ_{F^-} = 24.17\%$) > children ($HQ_{NO_3^-} = 23.00\%$ and $HQ_{F^-} = 10.55\%$) > teens ($HQ_{NO_3^-} = 13.16\%$ and $HQ_{F^-} = 2.00\%$) > adults ($HQ_{NO_3^-} = 11.62\%$ and $HQ_{F^-} = 1.25\%$) (Table 3).

The deterministic and probabilistic *RCLs* (*HQ* > 1) indicate trivial non-carcinogenic risks from the indicator parameters (NO_3^- and F^-) through the dermal route. Therefore, the perusal of Table 3 shows that NO_3^- and F^- exposure through direct groundwater consumption has higher non-carcinogenic *HQ* by several orders of magnitude than that of the dermal route in all age groups. Liu get similar findings of non-cancerous health risks from the groundwater of Weining plain, China[72]. Further, among the indicator parameters, the mean, median and 95th percentile values of $HQ_{NO_3^-}$ are more than those of HQ_{F^-} through the groundwater ingestion pathway within each stratified age group in both deterministic and probabilistic approaches (Table 3).

Hazard index (HI)

The non-carcinogenic *HI* is the combination of non-carcinogenic hazard quotient risk factors of each indicator parameter (NO_3^- or F^-) through multi-exposure pathways (ingestion and dermal) of groundwater, as shown in Table 4. The mean, median and 95th percentile values of infants and children in the deterministic result exceed the safety reference level of $HI_{NO_3^-} > 1$, divulging prominent threat level of non-carcinogenic HHR from NO_3^- in these age groups. The remaining population groups (teens and adults) in deterministic study and all the target population groups in probabilistic estimate reveal the non-carcinogenic risk of NO_3^- at 95th percentile values only ($HI_{NO_3^-} > 1$).

With respect to F^-, in the deterministic study, the potential non-cancerous effect is prominent in infants since the mean, median and 95th percentile values are above the safe reference limit (i.e., $HI_{F^-} > 1$), but the rest of the subpopulation groups show $HI_{F^-} > 1$ in 95th percentile only, which shows that the threat of health risk is still persistent in the sensitive sections of the stratified age groups at the extreme value. On the other hand, in the probabilistic estimate, the HI_{F^-} results indicate that the infants and children's groups are at the risk of non-carcinogenic effect at 95th percentile values, i.e., $HI_{F^-} > 1$.

Accordingly, in the deterministic output, the *RCL* magnitude of non-carcinogenic $HI_{NO_3^-}$ risk stands at infants (51.85%) > children (48.15%) > teens (40.74%) = adults (40.74%), and that of HI_{F^-} at infants (66.67%) > children (37.04%) > adults (33.33%) > teens (25.23%) (Table 4). The probabilistically calculated *RCL* health risks in the subpopulation groups are in the following order: infants ($HI_{NO_3^-} = 34.03\%$ and $HI_{F^-} = 24.17\%$) > children ($HI_{NO_3^-} = 23.01\%$ and $HI_{F^-} = 10.56\%$) > teens ($HI_{NO_3^-} = 13.17\%$ and $HI_{F^-} = 2.00\%$) > adults ($HI_{NO_3^-} = 11.62\%$ and $HI_{F^-} = 1.25\%$).

The deterministic *RCL* for *HI* is more than the probabilistic *RCL* in all age groups divulging that the deterministic estimation is based on the extreme (single point) values (please see Table S1, fifth column) for all input variables individually at different concentration levels of the indicator parameters. Since these extreme (single point) values may not always represent the actual field conditions, the deterministic estimates often lead to overestimation of the output results (Table 4). Therefore, the deterministic approach cannot cater to the holistic scenario of risk assessment for the inclusive members of the population interests due to differences in person-to-person characteristics and dynamism prevailing in the environment.

The probabilistic approach gives a range of values to choose from depending on the most likelihood field conditions (please see Table S1, eighth column). Therefore, the probability approximation of events reduces the uncertainties by providing more accurate and prospective risk assessment outcomes than those of the conventional deterministic approach. Liu[72] too conclude that the health risk assessment in groundwater through probabilistic simulation provides more comprehensive results.

The present study, however, suggests that the HRA of the indicator parameters should be studied using both deterministic and probabilistic approaches mutually to obtain more holistic outputs, thereby reducing the uncertainties and overcoming the conservative risk analysis of the point estimation. In a similar line, Kaur[25] conclude that the deterministic and probabilistic methods may be studied independently to assess non-carcinogenic HHRA (NO_3^- and F^-) in groundwater.

Sensitivity and uncertainty analysis

Deterministic technique does not provide any provision for sensitivity and uncertainty analysis. Therefore, sensitivity analysis has been carried out in the probabilistic process of working using the Monte Carlo Simulation (MCS) approach to extract the most influential input variables for the non-carcinogenic risk prediction. Figure 3a,b represents the tornado plots showing the percentage scales of all input variables for non-carcinogenic $HI_{NO_3^-}$ and HI_{F^-} in the stratified age groups. The sensitivity analysis validates that the variables of dermal route are not vividly influenced in the overall contribution of non-carcinogenic HI in all subpopulation groups and that the input variables of the ingestion pathway have more potential non-carcinogenic health effects than those of the dermal contact. The HQ results are further supported and validated by the sensitivity analysis of tornado plots. For $HI_{NO_3^-}$ sensitivity output, the parameter concentration ($C_{M\ ingestion}$) is the most influential variable followed by exposure duration ($ED_{ingestion}$) with minor contributions from ingestion rate ($IR_{ingestion}$) and exposure frequency ($EF_{ingestion}$) in all target populations. It indicates that higher NO_3^- content in ingested water will have more health implications, but as per Carlsson[94], 60–70% of the intake NO_3^- dose is generally excreted within the first 23 h in urine. Therefore, possibly the clinical NO_3^- toxicity in humans is less significant because of the limited exposure duration of NO_3^- intake dose in the body.

The results of sensitivity analysis HI_{F^-} for infants and children stand in the order of $ED_{ingestion} > C_{M\ ingestion} > IR_{ingestion} > EF_{ingestion}$. In infants and children, 80% of the oral F^- intake is absorbed in the body with storage in the bones and[95]. Thus, exposure duration is the most significant input variable due to high retention of F^- intake dose in infants and children. The tornado HI_{F^-} plots for teens and adults show the percentage of contribution variables as $C_{M\ ingestion} > ED_{ingestion} > IR_{ingestion} > EF_{ingestion}$. For teens and adults, ~ 50% of an orally ingested F^- is retained in the body[95,96]. Thus, the lower retention potential of F^- dose in teens and adults compared to that in infants and children indicates that the parameter concentration is the main driving force for fluoride toxicity in the sensitivity outputs. The body weight ($BW_{ingestion}$) variable negatively infers non-carcinogenic $HI_{NO_3^-}$ and HI_{F^-} simulations in all age groups (Fig. 3a,b).

Uncertainty analysis is crucial in determining the conservatism, ramification, and certainty accuracy level of the risk analysis results[97]. In this study, the application of MCS is notably enhanced to identify and quantify the uncertainties in the non-cancer HRA. Nevertheless, there are still other uncertainties that remain unaccounted in the model input variables, thereby limiting the validity of the whole scenario study. For example, (i) the daily water intake and dermal contact of target population groups are not measured during the groundwater sampling, (ii) body weights of the local population are not evaluated (instead, the representative data of the Indian Council of Medical Research (ICMR) and USEPA are used), (iii) average time, dermal permeability and conversion factor are considered as the same, fixed or similar values for deterministic and probabilistic approaches for different age groups, (iv) the variables data to generate the probability distribution functions (PDFs) using MCS are acquired from the USEPA and other relevant published literatures, (v) assumption that the concentrations of specific chemical parameters in groundwater are fully bio-absorbed in the human body may lead to ambiguity in risk analysis, and finally (vi) the reference doses (RfD) for ingestion and dermal exposures are obtained from USEPA.

Hydrogeochemical processes

Gibbs diagram is applied to elucidate the mechanism controlling groundwater chemistry in the study area[98]. This diagram enables understanding of the relationship between cation ratio [$Na^+/(Na^+ + Ca^{2+})$] or anion ratio [$Cl^-/(Cl^- + HCO_3^-)$] versus TDS, thereby defining three distinct areas, namely evaporation, rock-water and precipitation zones (Fig. 4) that depicts that majority of the groundwater samples (88.89%) are clustered in the rock dominance zone and the remaining samples (11.11%) fall in the evaporation zone.

Groundwater chemistry is primarily influenced by various geochemical processes, especially the interaction of percolating water with subsurface rocks and the chemical solute exchange processes of aquifer minerals in the study area. Many researchers conclude that the elevated concentrations of F^- in groundwater are proportionately related to rock-water interaction[99–102]. Besides the rock weathering processes, climatic factors too play a critical role in regulating the evaporation in the semiarid region[26]. The scattering of samples in the Gibbs diagram signifies the impact of anthropogenic inputs in the aquifer systems. The role of the evaporation factor enhances the groundwater salinity by elevating the Na^+ and Cl^- ions, resulting in the higher TDS concentrations, which are further abetted by anthropogenic activities[103].

Piper diagram is a widely used graphical interpolation to characterize the hydrochemical interaction, water genesis and groundwater contamination sources[29,104,105]. Figure 5 depicts that the groundwater is predominantly dominated by alkaline earths over the alkalies and weak acids over the strong acids. This is represented by three hydrochemical facies, namely $Ca^{2+}–Mg^{2+}–HCO_3^-$ (55.56%), $Ca^{2+}–Mg^{2+}–Cl^-–SO_4^{2-}$ (29.63%) and $Na^+–K^+–HCO_3^-$ (14.81%). Also, the groundwater samples are further classified into four water types, i.e., $Ca^{2+}–HCO_3^-$ (55.56%), $Ca^{2+}–Cl^-$ (7.40%), $Ca^{2+}–Mg^{2+}–Cl^-$ (22.22%) and $Ca^{2+}–Na^+–HCO_3^-$ (14.81%). The highest percentage of $Ca^{2+}–HCO_3^-$ water type indicates dissolution of carbonate minerals with percolating water from irrigation runoff and precipitation in the subsurface aquifers[11,76]. The cations triangle shows that majority of the samples (70.37%) belong to no-dominant zone, and the remaining samples of 11.11%, 14.82% and 3.70% represent water types in Ca^{2+}, Na^+ and Mg^{2+} dominated zones, respectively. In the anions triangle, around 70.37% samples fall in HCO_3^- water type, which indicates weathering of carbonates and silicates minerals and ion exchange
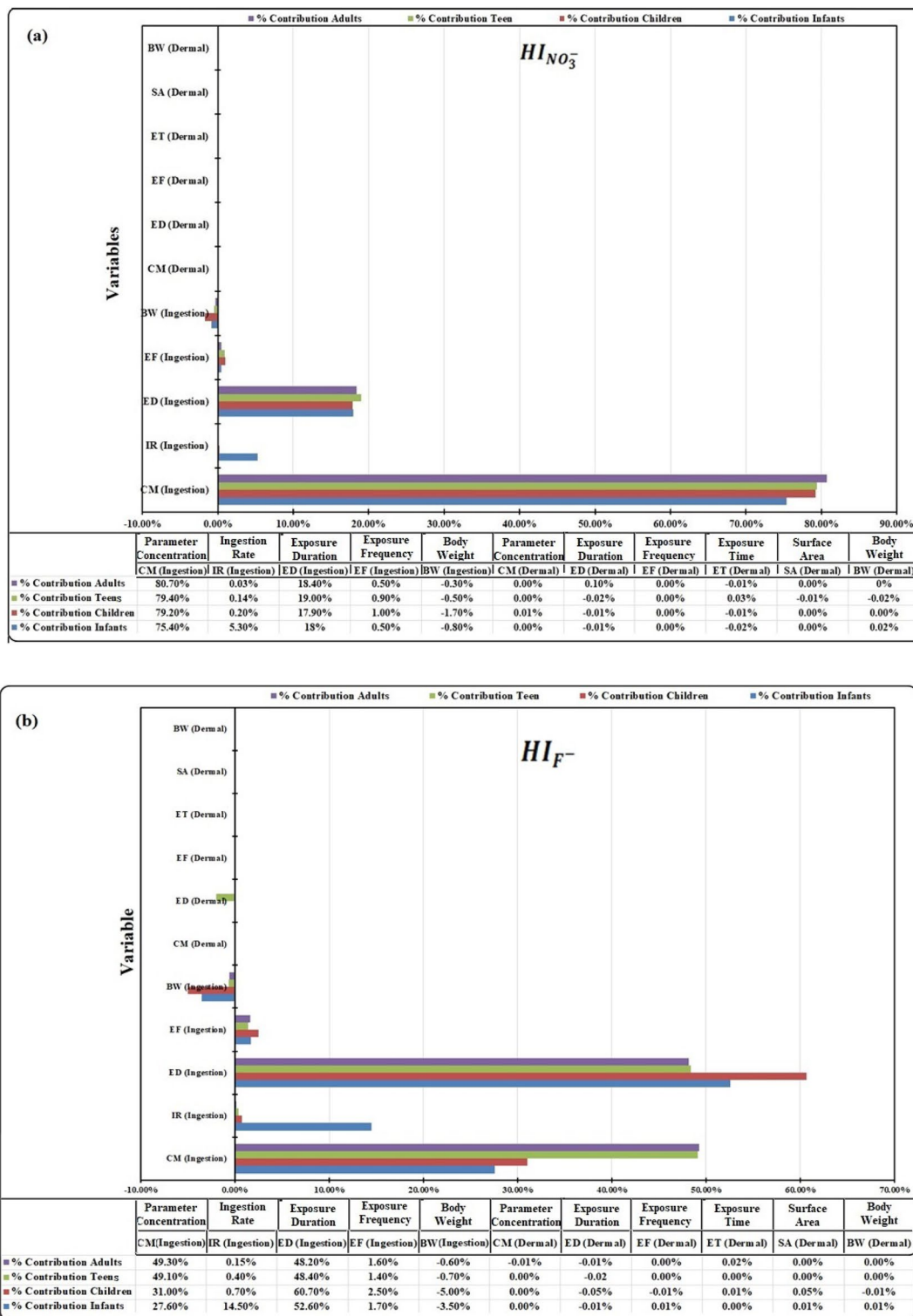
Figure 3. Tornado plots illustrating sensitivity analysis of input variables to the non-carcinogenic hazard index (*HI)* of groundwater: (**a**) NO$_3^-$ and F$^-$ ingestion and (**b**) for dermal contact: This sensitivity analysis figure is drawn by the probabilistic approach using the Monte Carlo Simulation (MCS) technique to extract the most influential input variables for the non-carcinogenic risk prediction for human health. The length of horizontal bars indicates the percentage contribution of various input variables to extract the non-carcinogenic hazard index (*HI)* of different age groups.
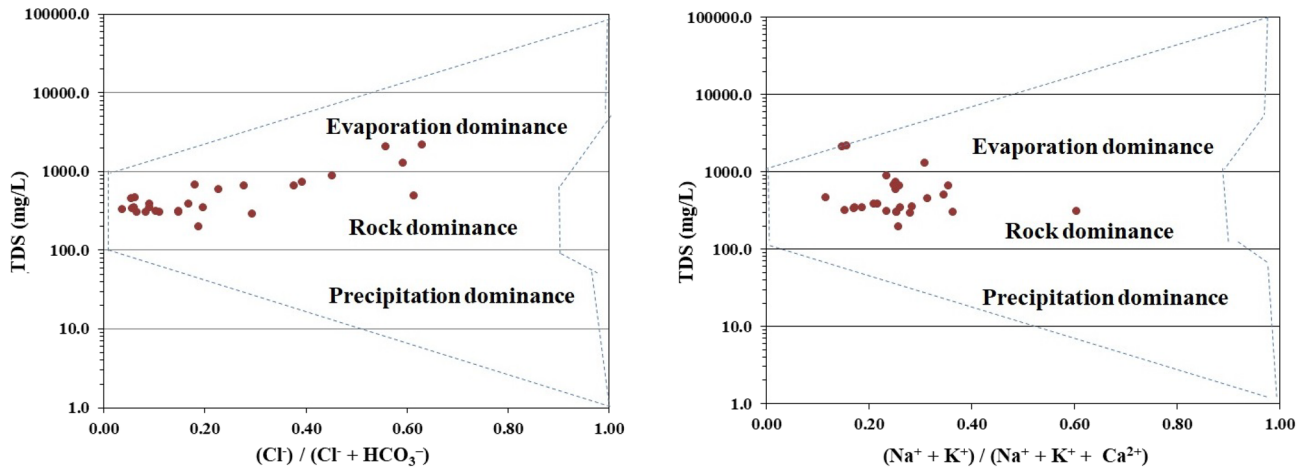
Figure 4. Gibbs diagram representing the factors controlling groundwater chemistry: This diagram enables to understand the relationship between cation ratio $[Na^+/(Na^+ + Ca_2^+)]$ or anion ratio $[Cl^-/(Cl^- + HCO_3^-)]$ versus TDS defining three distinct areas, namely evaporation, rock-water and precipitation zones to elucidate the dominant mechanism influencing the groundwater chemistry of the study area.
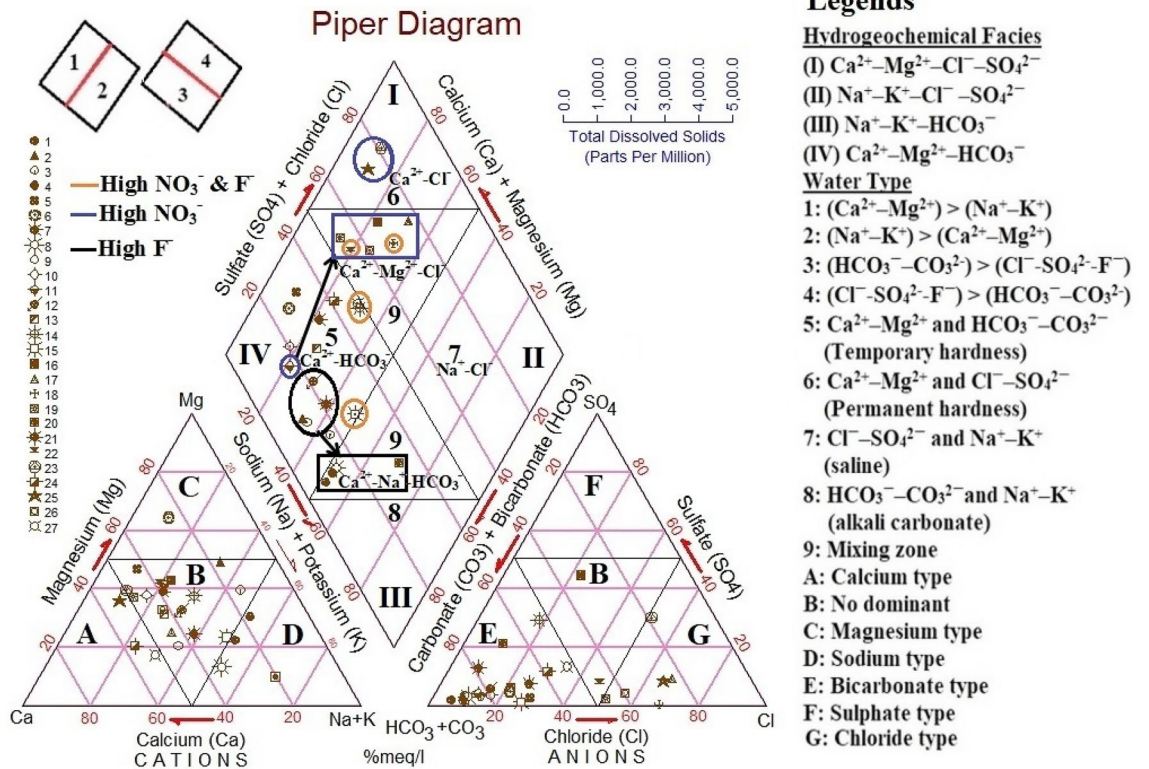

Figure 5. Piper diagram illustrating hydrochemical facies and water types: This graphical interpolation enables characterization of the hydrochemical interaction, genesis of water and groundwater contamination sources. Black arrows signify the conversion of water types due to anthropogenic and geogenic factors.

processes in the groundwater[106]. Approximately 22.22% of the samples belonging to Cl^- water type depict the role of anthropogenic factors and dissolution of evaporities in the groundwater[26]. The transformation of water types from $Ca^{2+}-HCO_3^-$ to $Ca^{2+}-Cl^-$ and $Ca^{2+}-Mg^{2+}-Cl^-$ types divulges the adverse impacts of human activities and applications of N-chemicals on cultivated lands, thereby elevating the NO_3^- concentrations in groundwater[107,108]. Further, the conversion of water from $Ca^{2+}-HCO_3^-$ to $Ca^{2+}Mg^{2+}-Cl^-$ and $Ca^{2+}-Na^+-HCO_3^-$ types is due to the dissolution of fluorite minerals (CaF_2) and cation exchange between Ca^{2+} and Na^+[109,110]. Subba Rao suggests that the weathering of rocks, higher Na^+ and HCO_3^- (or $NaHCO_3$) and alkaline nature of water favour the gradual increase of F^- concentrations in groundwater[100,111].

Source apportionment and geochemical relationships of NO_3^- and F^- with other parameters
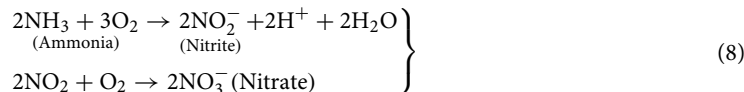
Many workers have studied the relationship of nitrate and fluoride with specific parameters through scatter plots. For example, for nitrate: NO_3^- versus pH[76], NO_3^- versus Cl[-17], NO_3^- versus K^+, NO_3^- versus Ca^{2+}, NO_3^- versus SO_4^{2-}, NO_3^- versus Cl[-112], NO_3^- versus EC, NO_3^- versus Cl^{-}, NO_3^- versus K^+, NO_3^- versus SO_4^{2-}, NO_3^- versus Na^+, NO_3^- versus Ca^{2+}, NO_3^- versus Mg^{2+}, NO_3^- versus HCO_3^{-27}, and for fluoride: F versus pH, F^- versus HCO_3^{-76}, F^- versus HCO_3^-, F^- versus Na^+, F^- versus NO_3^{-102}, F^- versus pH, F^- versus Ca^{2+113}, F^- versus pH, F^- versus Na^+, F^- versus K^+, F^- versus HCO_3^-, F^- versus Ca^{2+114}. However, these studies have not evaluated NO_3^- and F^- holistically for their geochemical relationships with physical parameters and major cations and anions and also their source apportionment with site-specific datasets available. The present study is unique in the sense that it uses scatter plots to correlate NO_3^- and F^- with other physicochemical parameters independently (pH, EC, TH, Ca^{2+}, Mg^{2+}, Na^+, K^+, Cl^-, HCO_3^-, SO_4^{2-}, and F^- versus NO_3) to achieve these objectives.

Source apportionment and geochemical relationship of NO_3^- with other parameters
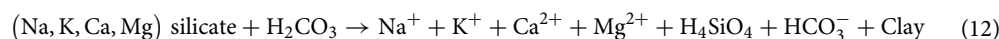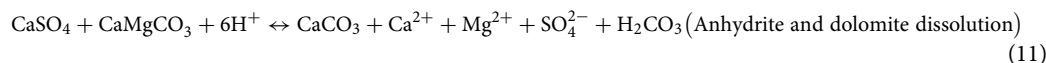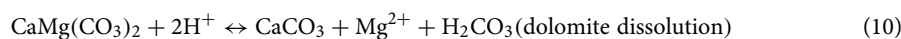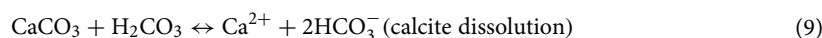
A strong inverse correlation between NO_3^- and pH ($r^2 = 0.688$ and $y = -0.0061x + 8.0993$) indicates decreasing pH values with increasing NO_3^- concentrations (Fig. 6a). Dadgar and Payandeh[115] too report this relationship in Tabriz province, Iran. The oxidation of dissolved CO_2 in groundwater forms carbonic acid and readily dissociates into H^+ and HCO_3^- ions is an intensive process[24]. Further, NO_3^- ions rapidly react with free H^+ ions to form HNO_3 resulting in acidic conditions at higher NO_3^- concentrations (Eq. 7).

$$\left.\begin{array}{l} CO_2 + H_2O \rightarrow H_2CO_3 \,(\text{Carbonic acid}) \\ H_2CO_3 \rightarrow H^+ + HCO_3^- \\ NO_3^- + H^+ \leftrightarrow HNO_3 \,(\text{Nitric acid}) \end{array}\right\} \tag{7}$$
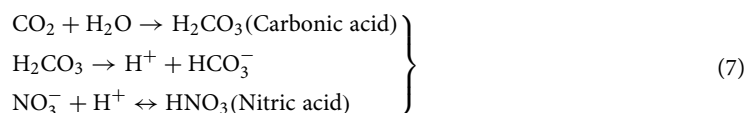
The scatter plot of NO_3^- versus EC shows a positive correlation ($r^2 = 0.5185$), divulging higher mineralization of dissolved substances, including excess NO_3^- concentrations in groundwater (Fig. 6b). The samples with NO_3^- contents above the guideline value of 45 mg/L[46] have higher EC in groundwater. Such a relationship is often associated with anthropogenic inputs, such as agricultural runoff, domestic sewage, poultry farming and unplanned urbanization, which release an enormous quantity of organic nitrogen and ammonia[76,116–118]. Ammonia is affectively absorbed in the soil particles that restrict its movement. During the limited aerobic condition in the soil, the nitrification process converts the immobilized ammonia into nitrate by bacterial activities, as shown in Eq. (8). Anthropogenic inputs accelerate the nitrification process that enhances easy leaching of NO_3^- from the soil in the percolating water recharging the aquifers.

$$\left.\begin{array}{l} 2NH_3 + 3O_2 \rightarrow 2NO_2^- + 2H^+ + 2H_2O \\ \quad \text{(Ammonia)} \qquad \text{(Nitrite)} \\ 2NO_2 + O_2 \rightarrow 2NO_3^- \,(\text{Nitrate}) \end{array}\right\} \tag{8}$$

The possible mineral source contributing Ca^{2+} and Mg^{2+} in the groundwater is determined by Ca^{2+}/Mg^{2+} ratio[119]. Figure 6d,e depicts the positive relationship of NO_3^- with Ca^{2+} ($r^2 = 0.6998$) and Mg^{2+} ($r^2 = 0.5672$), which indicates cation exchange processes in the groundwater due to prolonged application of N-fertilizers for crop production[120]. This cation exchange process significantly enhances the mineralization of Ca^{2+} and Mg^{2+} and elevates NO_3^- concentrations. Also, the nitrification process increases the NO_3^- level and acidity in groundwater resulting in Ca^{2+} and Mg^{2+} enrichment by the dissolution of carbonate minerals[76,121], as illustrated in Fig. S3a, i.e., 14.8% samples by dolomite and 48.2% by calcite in our study area. The remaining 37% samples have Ca^{2+}/Mg^{2+} ratio values > 2 depicting the influence of silicate weathering in groundwater[122]. The study area is a metamorphic terrain with a rich deposition of calcsilicate, hornblende, quartz and biotite[57]. Therefore, Ca^{2+} and Mg^{2+} concentrations in groundwater are influenced by carbonate and silicate rock-water interaction as expressed in Eqs. (9)–(12)[24,123–125].

$$CaCO_3 + H_2CO_3 \leftrightarrow Ca^{2+} + 2HCO_3^- \,(\text{calcite dissolution}) \tag{9}$$

$$CaMg(CO_3)_2 + 2H^+ \leftrightarrow CaCO_3 + Mg^{2+} + H_2CO_3 \,(\text{dolomite dissolution}) \tag{10}$$

$$CaSO_4 + CaMgCO_3 + 6H^+ \leftrightarrow CaCO_3 + Ca^{2+} + Mg^{2+} + SO_4^{2-} + H_2CO_3 \,(\text{Anhydrite and dolomite dissolution}) \tag{11}$$

$$(Na, K, Ca, Mg) \text{ silicate} + H_2CO_3 \rightarrow Na^+ + K^+ + Ca^{2+} + Mg^{2+} + H_4SiO_4 + HCO_3^- + Clay \tag{12}$$

Since NO_3^- has a strong positive loading with Ca^{2+} and Mg^{2+}, it exhibits a significant positive correlation with TH ($r^2 = 0.7247$) (Fig. 6c). Water hardness is attributed to the elevated concentrations of dissolved alkaline earth elements (Ca^{2+} and Mg^{2+}) in the aquifer system[79]. The scatter plots of NO_3^- with Na^+ ($r^2 = 0.085$) (Fig. 6f) and K^+ ($r^2 = 0.0627$) (Fig. 6g) signify a very weak positive relationship and suggest that the anthropogenic inputs are not the only primary source of alkali ions contents in groundwater. The bivariate plot of $Na^+ + K^+$ versus TZ^+ (Fig. S3b) depicts that the entire groundwater samples fall below the 1:1 aquiline. This indicates the weathering effect of silicate minerals besides the anthropogenic impacts, such as the application of NPK fertilizers and discharge of untreated sewerage water on the open ground, which elevate the Na^+ and K^+ concentrations in
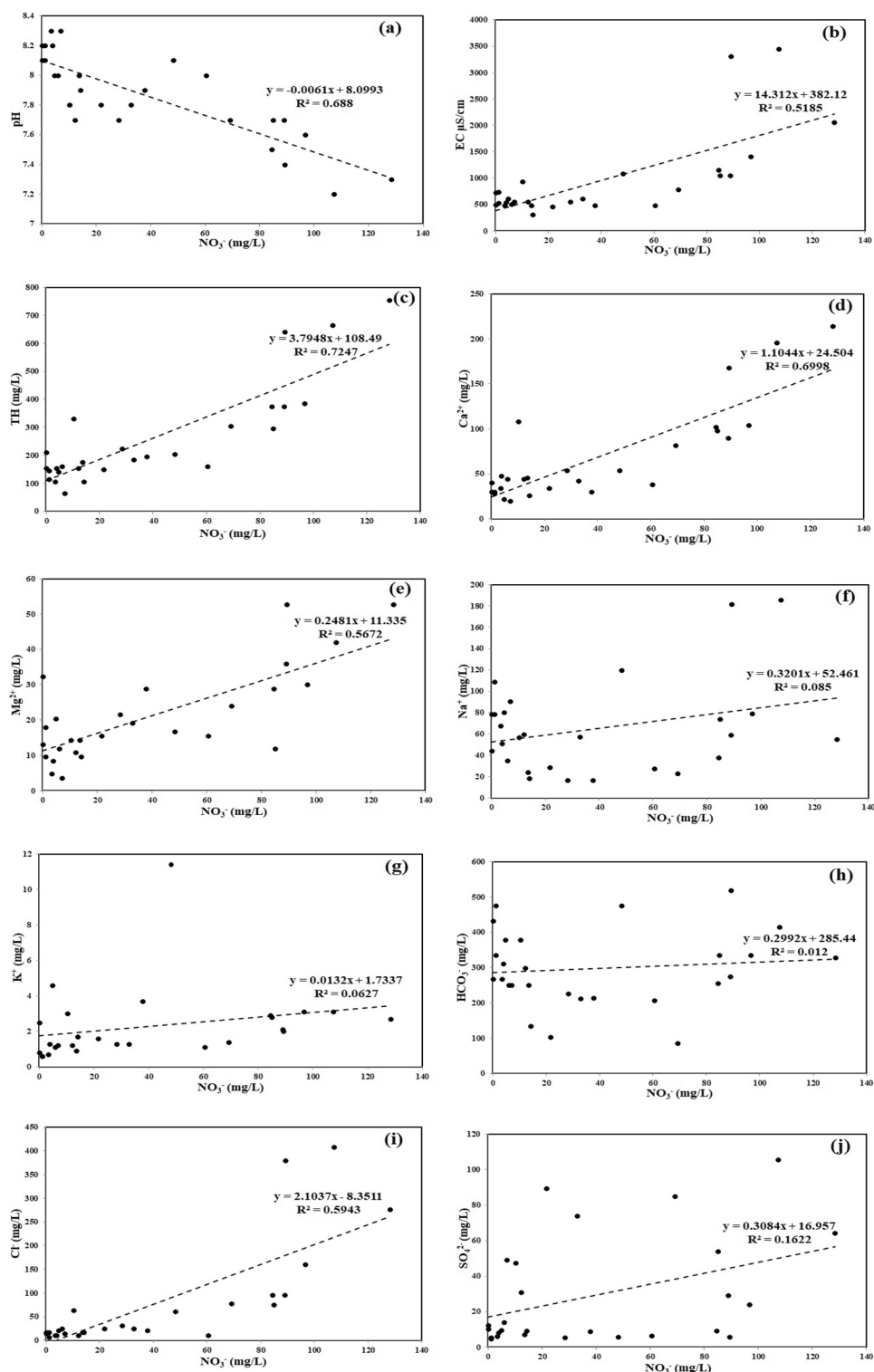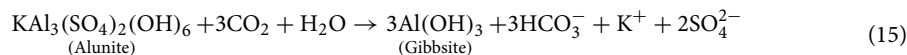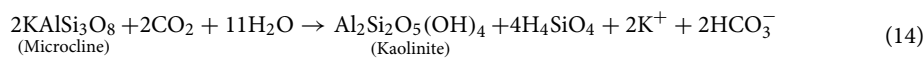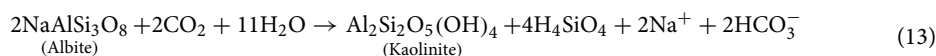
Figure 6. Scatter plot correlations between NO_3^- and (**a**) pH, (**b**) EC, (**c**) TH, (**d**) Ca^{2+}, (**e**) Mg^{2+}, (**f**) Na^+, (**g**) K^+, (**h**) HCO_3^-, (**i**) Cl^-, (**j**) SO_4^{2-} in groundwater samples: Each plot signifies the relationship of NO_3^- with a particular physicochemical parameter to understand their geochemical interaction. Source apportionment of NO_3^- is carried out with the help of such interactions.

groundwater[11,27,126,127]. In the study area, albite, microcline and alunite dissolution are the key sources of Na^+ and K^+ ions through rock-water interactions, as shown in Eqs. (13)–(15).
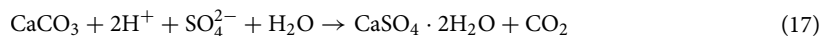
14

$$2NaAlSi_3O_8 + 2CO_2 + 11H_2O \rightarrow Al_2Si_2O_5(OH)_4 + 4H_4SiO_4 + 2Na^+ + 2HCO_3^- \tag{13}$$
(Albite)   (Kaolinite)

$$2KAlSi_3O_8 + 2CO_2 + 11H_2O \rightarrow Al_2Si_2O_5(OH)_4 + 4H_4SiO_4 + 2K^+ + 2HCO_3^- \tag{14}$$
(Microcline)   (Kaolinite)

$$KAl_3(SO_4)_2(OH)_6 + 3CO_2 + H_2O \rightarrow 3Al(OH)_3 + 3HCO_3^- + K^+ + 2SO_4^{2-} \tag{15}$$
(Alunite)   (Gibbsite)

The scatter plot of NO_3^- versus HCO_3^- shows the least positive loading ($r^2 = 0.012$) among the anions (Fig. 6h). This relationship suggests that the HCO_3^- does not exhibit much variation with increasing or decreasing NO_3^- concentrations. The fact that HCO_3^- ions are the dominant anions in the groundwater samples confirms that its primary source is possibly carbonate and silicate weathering[26,76,122,128], as shown in Eqs. (9)–(12).

In NO_3^- versus Cl^- plot (Fig. 6i), their positive correlation ($r^2 = 0.5943$) implies a common source, such as a combination of oxidation of animal and human waste[44], application of manure and nitrogenous fertilizers[129], septic tank seepages[130], agricultural runoff[131], etc. Similar findings are reported in the semiarid regions of many Indian States, such as Punjab[24], Rajasthan[132], Andhra Pradesh[133], and Telangana[134].

Figure 6j depicts the weak positive loading between NO_3^- and SO_4^{2-} ($r^2 = 0.1622$) due to two separate sets of NO_3^- and SO_4^{2-} concentrations in the groundwater samples. The samples having low or high NO_3^- levels have both low and high SO_4^- concentrations, thus neglecting the influence of the anthropogenic activities on SO_4^{2-}.

The plot of Ca^{2+} versus SO_4^{2-} (Fig. S3c) is meant to identify the minerals that contribute to higher amount of Ca^{2+} and SO_4^{2-} ions in groundwater[76]. Majority of the samples (92.6%) are below the equiline (1:1), indicating that the role of gypsum ($CaSO_4 \cdot 2H_2O$) dissolution is insignificant. The remaining samples (7.4%) falling along the equiline depict the dissolution of anhydrite ($CaSO_4$) mineral in the groundwater[135,136]. The gypsum precipitation in the groundwater occurs through direct hydration of anhydrite and dissolution of calcium-bearing minerals oxidized with sulphate and hydronium ions[137], as expressed in Eqs. (16) and (17). Hence, the weak positive correlation between Ca^{2+} and SO_4^{2-} ($r^2 = 0.197$) (Fig. S3c) suggests that the limited concentrations of Ca^{2+} ions in the groundwater may be due to the precipitation of gypsum[138]. If the study area lacks gypsum mineral, then the biologically oxidized sulphur containing compounds deposited by the rainwater and nitrogen compounds in the soil leach down to groundwater as SO_4^{2-} and NO_3^- ions[139]. Thus, the positive regression line between NO_3^- and SO_4^{2-} ($y = 0.3084x + 16.957$) (Fig. 6j) is found in the groundwater samples of the study area. Karunanidhi[27] report similar findings on the positive relationship between NO_3^- and SO_4^{2-} in the groundwater samples of Tiruppur region, India. Moreover, the dissolution of alunite [$KAl_3(SO_4)_2(OH)_6$], as expressed in Eq. (15), will also contribute to the SO_4^{2-} ions in groundwater.

$$CaSO_4 + 2H_2O \rightarrow CaSO_4 \cdot 2H_2O \tag{16}$$

$$CaCO_3 + 2H^+ + SO_4^{2-} + H_2O \rightarrow CaSO_4 \cdot 2H_2O + CO_2 \tag{17}$$

Source apportionment and geochemical relationship of F^- with other parameters

Normally, high pH in groundwater depicts its alkaline nature, resulting in elevated concentrations of HCO_3^- and high hydroxyl (OH^-) ions (Eq. 18, Tables 2 and S2, Fig. S2). A fairly positive relationship between pH and F^- ($r^2 = 0.2607$; Fig. 7a) indicates that the alkaline water favours dissolution and mobilization of F^- bearing minerals in groundwater[140]. The weathering processes of fluoride-bearing rocks to replace F^- ions with OH^- ions in the lattices of different minerals, namely muscovite, biotite, amphibole, and hornblende, has enriched the F^- concentrations in groundwater. Xiao[141] and Karunanidhi[142] express the displacement mechanism of F^- ions by OH^- ions in the muscovite, biotite, and hornblende minerals as follows (Eqs. 19–21).

$$HCO_3^- + H_2O = H_2CO_3 + OH^- \tag{18}$$

$$KAl_2[AlSi_3O_{10}]F_2 + 2OH^- = KAl_2[AlSi_3O_{10}](OH)_2 + 2F^- \tag{19}$$

$$KMg_3[AlSi_3O_{10}]F_2 + 2OH^- = KMg_3[AlSi_3O_{10}](OH)_2 + 2F^- \tag{20}$$

$$NaCa_2(Mg, Fe, Al)_5(Al, Si)_8O_{22}F_2 + 2OH^- \rightarrow NaCa_2(Mg, Fe, Al)_5(Al, Si)_8O_{22}(OH)_2 + 2F^- \tag{21}$$
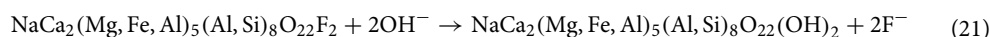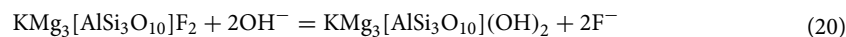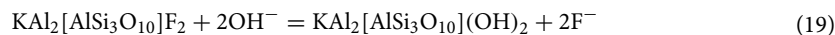
Figure 7b shows a negative trend between the EC and F^- ($r^2 = 0.0118$; $y = -147.3x + 1079$), indicating no major influence of EC on F^- ion concentrations. A rather weak, but negative relationship of F^- with Ca^{2+} ($r^2 = 0.1262$, $y = -31.957x + 97.575$) and Mg^{2+} ($r^2 = 0.0922$, $y = -6.8172x + 27.41$) indicates decreasing concentrations of Ca^{2+} and Mg^{2+} ions in groundwater with increasing F^- content (Fig. 7d,e). Various workers report similar findings between F^- versus Ca^{2+} elsewhere[53,110]. The excess concentrations of HCO_3^- with high pH contribute to the alkaline water, thus favouring the dissolution of fluorite (CaF_2) in groundwater due to precipitation of $CaCO_3$[143], as shown in Eq. (22).
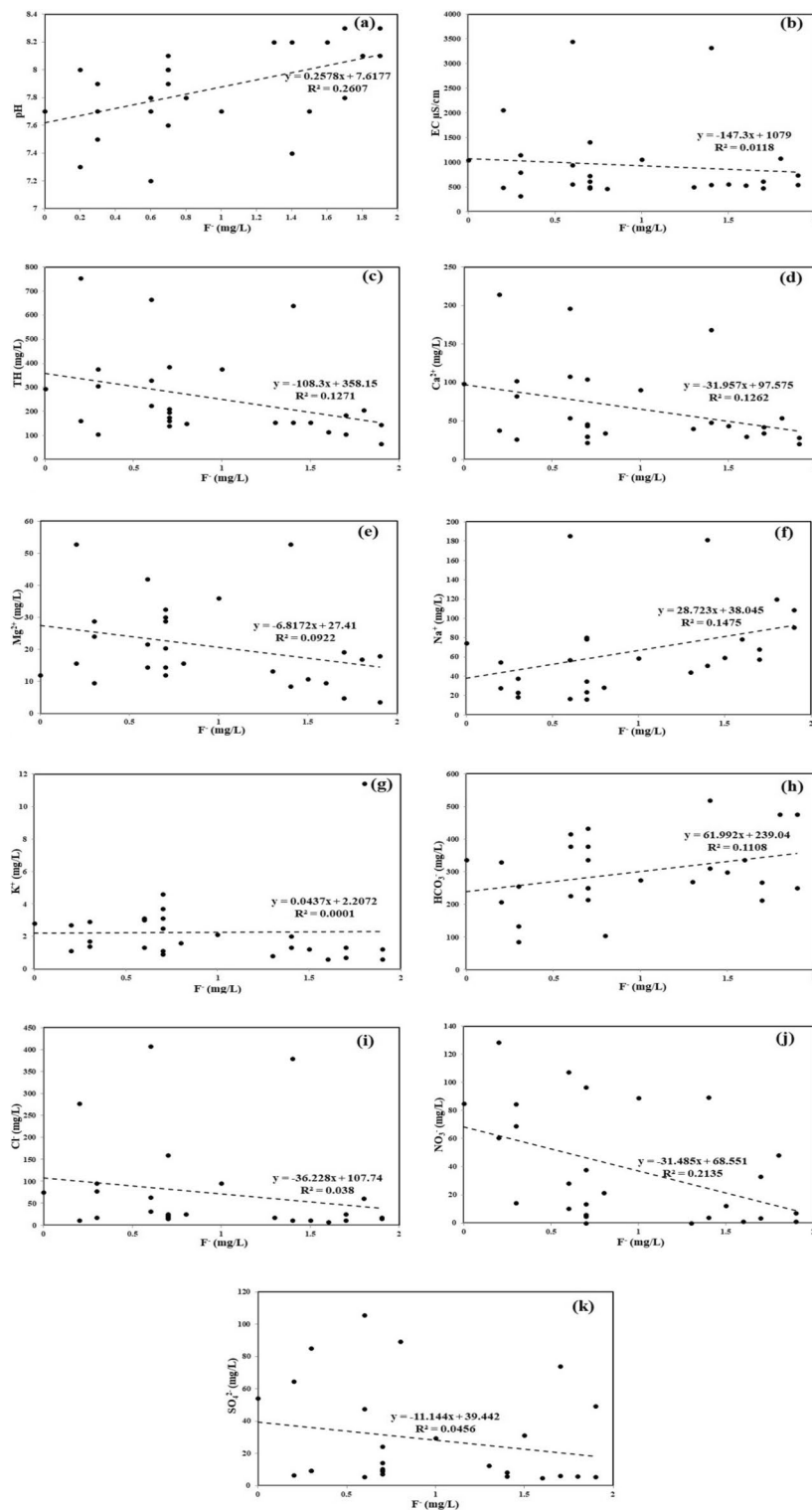
$$CaF_2 + 2HCO_3^- = CaCO_3 + 2F^- + H_2O + CO_2 \tag{22}$$
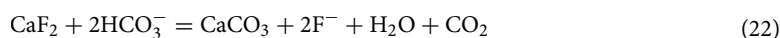
Figure 7. Scatter plot correlations between F⁻ and (**a**) pH, (**b**) EC, (**c**) TH, (**d**) Ca²⁺, (**e**) Mg²⁺, (**f**) Na⁺, (**g**) K⁺, (**h**) HCO₃⁻, (**i**) Cl⁻, (**j**) NO₃⁻, (**k**) SO₄²⁻ in groundwater samples: Each plot signifies the relationship of F⁻ with a particular physicochemical parameter to understand their geochemical interaction. Source apportionment of F⁻ is carried out with the help of such interactions.

Jack suggests that the rock-water interaction of fluoride-bearing minerals from a recharge area through the facture zone would precipitate the Ca²⁺ and Mg²⁺ ions as calcite, Mg-Calcite dolomite, and dolomite fluorite,

respectively, along the groundwater flow path to a discharge area[144]. Hem states that because Ca^{2+} and Mg^{2+} ions are divalent cations with similar properties, they possess the same stability with other ion pairs (SO_4^{2-}, CO_3^{2-} and HCO_3^-) and contribute similarly to water hardness[145]. Thus, the inverse relationship between TH and F^- (Fig. 7c) is due to decreased Ca^{2+} and Mg^{2+} ion concentrations or precipitation of calcium carbonate and Mg-calcite dolomite causing enhanced solubility of fluoride-bearing minerals in the study area[139,146].

While examining the role of Na^+, it is found that the Na^+/Ca^{2+} ratio helps in understanding the probable reason for lowering of Ca^{2+} activity in groundwater[144]. Around 37% of water samples have Na^+/Ca^{2+} ratio > 1, indicating that evapotranspiration is possibly affecting the Ca^{2+} activity by precipitating it and increasing the Na^+ concentrations, thus favouring the enrichment of F^- content in groundwater (Fig. S3d). The study area is a semi-arid region characterized by drier climatic conditions where the dissolved constituents are readily concentrated and precipitated by evaporation, thereby leading to groundwater salinity[147,148]. The remaining 63% groundwater samples show Na^+/Ca^{2+} ratio < 1, which depicts that rock-water interaction is another key contributing factor of generation of Ca^{2+} and F^- ions due to the dissolution of fluorite minerals in the groundwater. However, Ca^{2+} ions subsequently react with $NaHCO_3$ to form $CaCO_3$ precipitation (Eq. 23). In a similar line, Arveti[99] report that high F^- content in groundwater is directly related to the dissolution of fluoride enriched minerals due to prolonged residence time of water due to physiographic conditions or low hydraulic conductivity in aquifers providing a longer contact period. The plot Na^+ versus F^- ($r^2 = 0.1475$) with a positive slope ($y = 28.723x + 38.045$) indicates gradual increase of F^- concentrations with elevated Na^+ content in groundwater (Fig. 7f). The higher concentrations of $NaHCO_3$ or Na^+ ions with alkaline pH in groundwater allows dissolution of F^- ions from fluorite (CaF_2) through rock–water interaction[143,149] (Eq. 23).

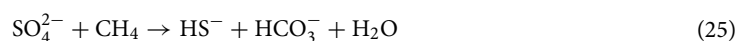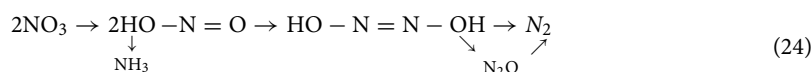$$CaF_2 + 2NaHCO_3 = CaCO_3 + 2Na^+ + 2F^- + H_2O + CO_2 \tag{23}$$
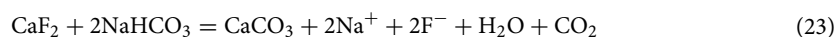
In Fig. 7g, the plot K^+ versus F^- divulges that there is no significant positive or negative relationship between them. The flat linear regression ($r^2 = 0.0001$) indicates that the K^+ does not have much influence on the fluoride mineralization in groundwater. The orthoclase feldspar ($KAlSiO_3O_8$) is generally resistant to attack by water, but apparently gets altered to silica, clay, and K^+ ions[145]. In the study area, rapid precipitation of alunite occurs in the aquifers due to the high degree of stability of potassium-bearing alumino-silicate minerals resulting in low content of K^+ in groundwater.

The positive trend between HCO_3^- and F^- ($r^2 = 0.1108$; $y = 61.992x + 239.04$) divulges that the increase in HCO_3^- content supports the dissolution of F^- bearing minerals in groundwater (Fig. 7h). However, few samples have low HCO_3^- concentrations with high F^- values which indicates that the F^- enrichment in groundwater is affected by a combination of processes, such as evapotranspiration and calcite precipitation[150]. The HCO_3^-/Ca^{2+}ratio predicts the likelihood of F^- enrichment in groundwater[140]. About 85% of samples show HCO_3^-/Ca^{2+}ratio > 1 (Fig. S3e), signifying that groundwater hydrological conditions are still favourable for further enrichment of fluoride minerals in the study area with their saturation index prevailing in the order of -2.66 to -0.68 (undersaturated condition).

The application of phosphatic and chloride containing fertilizers are the main anthropogenic sources of high F^-, NO_3^- and Cl^- contamination in the groundwater[24,150]. Figure 7i,j shows inverse relationship of F^- with Cl^- ($r^2 = 0.038$, $y = -36.228x + 107.74$) and NO_3^- ($r^2 = 0.2135$, $y = -31.485x + 68.551$), respectively. These plots signify that F^- contamination in groundwater is from a different source than that of Cl^- and NO_3; thus, the role of agricultural inputs for F^- generation is neglected. In some cases, when the redox potential falls below a certain value in groundwater, the denitrification process of NO_3^- by the nitrate-reducing bacteria, accompanied by increased pH value, enhances the precipitation of Ca^{2+} resulting in the high F^- and HCO_3^- concentrations in water (Eq. 24)[139].

The inverse correlation between SO_4^{2-} and F^- ($r^2 = 0.0456$; $y = -11.144x + 39.442$) indicates two different sets of SO_4^{2-} and F^- contents in the groundwater samples (Fig. 7k). The samples having low or high F^- levels have both low and high SO_4^- concentrations, thus neglecting the influence of anthropogenic activities. In groundwater, when the redox potential is below a specific value due to high evapotranspiration, sulphate-reducing bacteria initiate desulphurisation process that results in the loss of SO_4^{2-} ions (Eq. 25). Further, the desulphurisation process raises the pH value, thus favouring the fluorite solubility leading to the high concentrations of F^- and HCO_3^- ions and precipitation of Ca^{2+} ions as $CaCO_3$ in groundwater[139]. Many researchers have observed similar relationship between SO_4^{2-} versus F^- elsewhere[144,150,151], because the decrease in solubility of fluorite minerals is affected by the presence of SO_4^{2-} ions in groundwater.

$$2NO_3 \rightarrow \underset{NH_3}{2HO-N=O} \rightarrow HO-N=N-OH \rightarrow \underset{N_2O}{N_2} \tag{24}$$

$$SO_4^{2-} + CH_4 \rightarrow HS^- + HCO_3^- + H_2O \tag{25}$$

Chemometric analysis

Principal component analysis

Principal component analysis (PCA) is applied on the 13 chemical parameters to extract the significant principal components (PCs) that define the hydrogeochemistry in the study area and help in identifying the probable sources of these parameters in groundwater. A scree plot is generated to determine the eigenvalues of the PCs using the varimax rotation method. Three PCs were considered as significant from the entire extracted PCs whose eigenvalues are greater than 1. The eigenvalue of PC1, PC2 and PC3 are 57.60, 18.60 and 9.90, respectively, and their cumulative variance is 86.10% of all analyzed parameters (Table 5). The significant PCs having parameters loading scores of > 0.75 (strong, marked bold) and between 0.50 and 0.75 (moderate, marked bold with italics)

are considered for the PCA interpretation. The first principal component (PC1) that explains 57.60% of the cumulative variance shows strong positive loading on EC, TDS, TH, Ca^{2+}, Mg^{2+}, Cl^- and NO_3^- and a strong inverse relationship with pH (Table 5).

The loading TH (0.98) is directly related to Ca^{2+} (0.96) and Mg^{2+} (0.86) scores that indicate that water hardness is influenced by the alkaline earths concentrations in aquifers[77,104]. The weathering and dissolution of carbonate (calcite and dolomite) and silicate minerals through rock-water interaction are the probable sources of Ca^{2+} and Mg^{2+} in groundwater, which is also supported by Ca^{2+}/Mg^{2+} ratio[24]. The weak loading of alkalis (Na^+: 0.45 and K^+: 0.18) with respect to alkaline earths (Ca^{2+} and Mg^{2+}) supports the cation ion exchange process in groundwater[79].

Both Cl^- (0.93) and high loading of NO_3^- (0.90) indicate the effect of agrochemicals and domestic sewage in groundwater[29,152]. The application of chemical fertilizers, namely anhydrous ammonium chloride, ammonium nitrate and urea containing inorganic chlorine and nitrogen, is a matter of concern[11]. The inverse loading of pH (-0.92) is due to the oxidation of dissolved CO_2 and organic matter forming carbonic acids, thereby releasing free H^+ ions[153]. The inorganic chlorine and nitrogen react with H^+ ions rapidly to form HCl and HNO_3, which decrease pH in groundwater. The high scores of EC (0.89) and TDS (0.89) are due to the elevated concentrations of Ca^{2+}, Mg^{2+}, Cl^- and NO_3^- ions, which enhance the mineralization of groundwater in the study area. Therefore, PC1 is controlled by lithogenic (Ca^{2+} and Mg^{2+}) and anthropogenic (Cl^- and NO_3^-) factors.

The second principal component (PC2) explains 18.60% of the total variance. It is positively weighed on Na^+ (0.85) and F^- (0.77), moderately weighed on HCO_3^- (0.74) and has insignificant loading on Ca^{2+} (0.10) indicating lithogenic sources of these elements (Table 5). PC2 indicates that the dissolution of fluoride-bearing minerals is influenced by the elevated concentrations of Na^+ and HCO_3^- or $NaHCO_3$ in the aquifer system. On the other hand, the weak correlation of Ca^{2+} with F^- (Fig. 7d) suggests that high Ca^{2+} content in groundwater inhibits fluoride mineralization at alkaline pH[25,154,155]). Therefore, PC2 deals with fluoride dissolution through rock-water interaction.

Lastly, in the principal component 3 (PC3), a variance of 9.90% depicts positive correlation with K^+ (high: 0.79) and HCO_3^- (moderate: 0.50), and negative loading on SO_4^{2-} (moderate: -0.59) (Table 5). The main sources of K^+ and HCO_3^- are the weathering of silicate, muscovite, biotite, and microcline minerals found in the study area. The negative score of SO_4^{2-} is due to the leaching of inorganic sulphides present in the sediments through percolating water, weathering of pyrite-sulphides bearing minerals, namely pyroxene, amphiboles, magnetite and olivine[156] and biological oxidation of sulphur containing compounds in soil[139]. The oxidation of these minerals present in the soil profile or subsurface layers is operated through oxygen transport, viz., convection process and direct exposure of air, because of lowering of groundwater levels through evapotranspiration and groundwater extraction[157]. Further, the inverse correlations of SO_4^{2-} with K^+ and HCO_3^- reflect the different minerals sources contributing to these ions in the aquifer system. The concentrations of K^+, HCO_3^- and SO_4^{2-} are well within the acceptable limits or guideline values of BIS[46] and WHO[45], thus indicating geogenic inputs.

Cluster analysis

Cluster analysis (CA) is employed on the 27 groundwater samples to create different clusters by grouping similar samples in the form of a dendrogram. The samples grouped in each cluster are marked by certain specific parameters controlling them. Therefore, the variation in the clusters can be identified by computing the average value of each parameter of the sample(s) within a cluster to assess the specific tracers for each cluster[82,86]. Figure 8

Variable	PC1	PC2	PC3	Communality
pH	**-0.92**	0.17	0.08	0.89
EC	**0.89**	0.42	0.03	0.98
TDS	**0.89**	0.42	0.03	0.98
TH	**0.98**	0.09	0.04	0.96
Ca^{2+}	**0.96**	*0.10*	-0.02	0.93
Mg^{2+}	**0.86**	0.06	0.17	0.78
Na^+	0.45	**0.85**	0.13	0.94
K^+	0.18	0.08	**0.79**	0.67
HCO_3^-	0.26	***0.74***	***0.50***	0.87
Cl^-	**0.93**	0.31	-0.02	0.97
SO_4^{2-}	0.49	-0.09	***-0.59***	0.59
NO_3^-	**0.90**	-0.17	0.09	0.85
F^-	-0.45	**0.77**	-0.07	0.81
Eigen values	7.48	2.41	1.29	11.19
% of variance	57.60	18.60	9.90	
Cumulative % of variance	57.60	76.20	86.10	
Probable identified sources	Mixed factors (lithogenic and anthropogenic inputs)	Fluoride dissolution through rock-water interaction	Weathering of bedrocks, evapotranspiration and groundwater extraction	

Table 5. Rotated varimax component matrix of the analysed groundwater samples around village Supebeda in Chhattisgarh State, India. Bold indicates strong loading between parameters. Bold-Italics indicates moderate loading between parameters. *PC* Principal component.

depicts three significant clusters $[(D_{limk}/D_{max}) * 100 < 105]$ from the dendrogram. Table 6 provides the average values of the groundwater parameters for each cluster. Cluster 1 (C1) is formed by the largest number of samples (G1, G4, G8, G9, G12, G20, G14, G21, G2, G3, G5, G6, G7, G10, G11, G13, G15) with highest values of pH and F^-, higher values of Na^+ and HCO_3^- and lowest value of Ca^{2+} that indicate fluoride enrichment. The average values of the parameters belonging to C1 are below their respective standard limits of BIS[46] and WHO[45], except for F^- (1.14) (Table 6). Thus, the groundwater quality of C1 is influenced by the dissolution of fluoride-bearing minerals and fits well with PC2.

Cluster 2 (C2) denotes the higher values of TDS, TH, Ca^{2+}, K^+, SO_4^{2-} and NO_3^- and the lowest value of F^-. The average values of TDS (627.47), TH (316.43), Ca^{2+} (88.29) and NO_3^- (65.11) are above the acceptable limits of BIS[46] due to their excess concentrations in samples G19, G22, G23, G24, G26, and G27 (Tables S2 and Table 6).
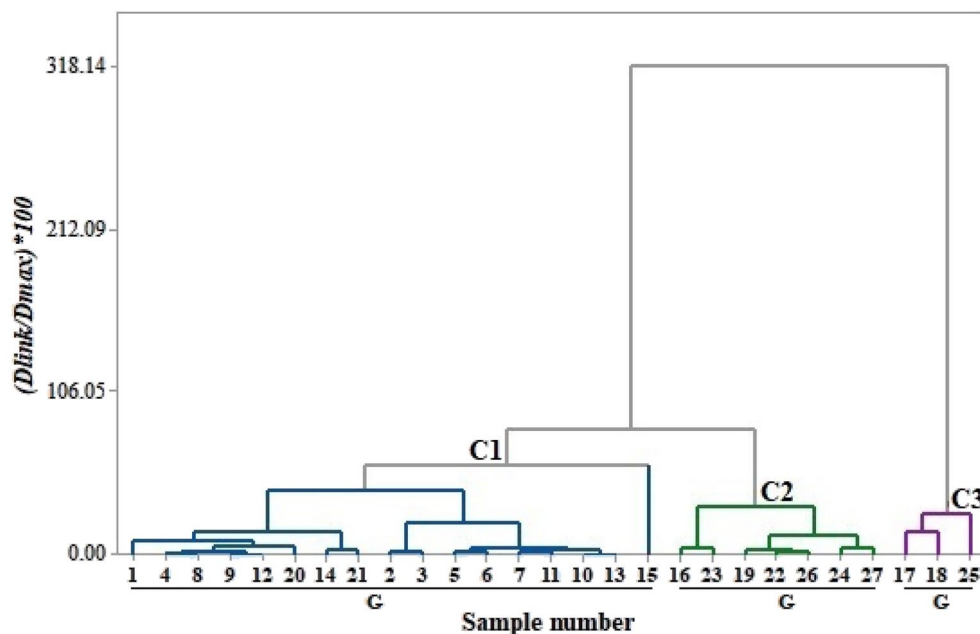

Figure 8. Dendrogram of groundwater sampling locations around village Supebeda in Chhattisgarh State, India: Three different clusters (C1, C2, and C3) are identified by Ward's method and the Euclidean distance to determine the similarity/dissimilarity. The relatively homogenous samples are grouped in each cluster and marked by certain specific parameters controlling them. In the y-axis, $(D_{limk}/D_{max}) * 100$ represents the quotient between the linkage distances for a particular case divided by the maximal linkage distance. The quotient is then multiplied by 100 to standardize the linkage distance represented by the y-axis.

Parameters	C1	C2	C3
pH	**8.03**	7.69	*7.30*
EC	572.00	980.43	**2939.67**
TDS	366.08	*627.47*	**1881.39**
TH	156.18	*316.43*	**686.67**
Ca^{2+}	*37.06*	*88.29*	**192.67**
Mg^{2+}	15.25	22.97	**49.20**
Na^+	*57.29*	51.17	**140.57**
K^+	2.12	*2.41*	**2.60**
HCO_3^-	*293.49*	252.86	**421.00**
Cl^-	19.66	84.73	**355.03**
SO_4^{2-}	15.82	*48.33*	**58.57**
NO_3^-	16.10	*65.11*	**108.27**
F^-	**1.14**	*0.53*	0.73

Table 6. Average values of the physicochemical parameters for each cluster. Bold indicates the highest average value of a parameter among the three clusters. Bold-Italics indicates the second highest average value of a parameter to identify the special tracer. Italics indicates the lowest average value of a parameter among the three clusters.

The lowest value of F⁻ (0.53) in C2 among the three significant clusters are due to only one sample (G22) that just touches the BIS[46] acceptable limit of F⁻ (Table S2). The groundwater samples (G16, G23, G19, G22, G26, G24, G27) that represent the C2 have K⁺ and SO_4^{2-} concentrations below their respective guideline values of WHO[45] and BIS[46]. Therefore, C2 is influenced by both geogenic and anthropogenic factors.

Finally, C3 is the smallest cluster (G17,G18,G25) and is marked by the highest values of EC, TDS, TH, Ca^{2+}, Mg^{2+}, Na^+, K^+, HCO_3^-, Cl^-, SO_4^{2-} and NO_3^- and the lowest value of pH (Table 6). The average values of EC (2939.67), TDS (1881.39), TH (686.67), Ca^{2+} (192.67), Mg^{2+} (49.20), Cl^- (355.03) and NO_3^- (108.27) are above their respective guideline or acceptable limits of BIS[46] and WHO[45], except for Na^+ (140.57), K^+ (2.60), HCO_3^- (421.00) and F⁻ (0.73), due to their elevated contents in sample numbers G17,G18 and G25 that decrease the pH in groundwater. On the other hand, only sample G18 has excess concentrations of HCO_3^- and F⁻ above their acceptable limits defined by BIS[46] (Table S2). Therefore, the specific parameters that majorly influence the C3 are EC, TDS, TH, Ca^{2+}, Mg^{2+}, Na^+, K^+, Cl^- and NO_3^- that indicate geogenic and anthropogenic inputs enhancing the mineralization of groundwater. Finally, C2 and C3 correspond to the combination of PC1 and PC3.

Conclusions

This paper highlights the non-carcinogenic human health risk assessment (HHRA) of NO_3^- and F⁻ contamination in groundwater on four different age groups (infants, children, teens and adult) through ingestion and dermal contact using deterministic and probabilistic approaches, source apportionment of NO_3^- and F⁻ with multiple parameters and chemometric modelling to extract the latent factors controlling the groundwater chemistry. Results of the deterministic and probabilistic hazard quotients (HQ) of nitrate ($HQ_{NO_3^-}$) and fluoride (HQ_{F-}) signify that the ingestion pathway has the potential non-carcinogenic health implications on all target populations. The deterministic results of the risk certainty levels (RCL) of the hazard index (HI) above unity for nitrate ($HI_{NO_3^-}$) stand at infants (51.85%) > children (48.15%) > teens (40.74%) = adults (40.74%) and for fluoride (HI_{F-}) at infants (66.67%) > children (37.04%) > adults (33.33%) > teens (25.23%). However, the probabilistically calculated RCL health risks in the subpopulation groups are in the order of infants ($HI_{NO_3^-}$ = 34.03% and HI_{F-} = 24.17%) > children ($HI_{NO_3^-}$ = 23.01% and HI_{F-} = 10.56%) > teens ($HI_{NO_3^-}$ = 13.17% and HI_{F-} = 2.00%) > adults ($HI_{NO_3^-}$ = 11.62% and HI_{F-} = 1.25%). These figures reveal that there exist higher degrees of potential human health risks in all the subpopulation groups in the deterministic outputs compared to those of the probabilistic model. Field observations do not support deterministic conclusions, but they do approve the probabilistic RCL values. This may be because the deterministic estimation is based on the assumption of an extreme (single point) value for all input variables individually at different concentration levels of the indicator parameters, thus possibly leading to overestimation of the output results since the extreme value may not represent the actual field conditions. Also, since the deterministic approach does not have any provision for validation of its output results, the analysis coming out of it is speculative by nature. On the contrary, the probabilistic approach provides options to choose from a range of values depending on the most likelihood field conditions besides a provision for sensitivity analysis, which enables validation of the input variables affecting the output results among the various exposure pathways. Due to all these considerations, this study concludes that probabilistic modelling is superior to deterministic approaches in human health risk assessment.

Strong positive correlation of scatter plots between NO_3^- with multiple parameters (EC, TH, Ca^{2+}, Mg^{2+} and Cl^-) indicate anthropogenic inputs, such as domestic sewage, agricultural runoff, oxidation of poultry wastes, etc. Prolonged application of N fertilizers has developed cation exchange processes between NH_3 and Ca^{2+} and Mg^{2+} enhancing the mineralization of Ca^{2+} and Mg^{2+} in groundwater, thus leading to water hardness and elevated NO_3^- concentrations. The positive regression lines between F⁻ and pH, Na^+ and HCO_3^-, respectively, infer that the alkaline pH with higher concentrations of $NaHCO_3$ or Na^+ or HCO_3^- ions in groundwater allows dissolution of fluoride-bearing rocks, such as muscovite, biotite, amphibole, fluorite, and hornblende through rock-water interaction. Therefore, the fact that about 85% of samples show HCO_3^-/Ca^{2+} ratio > 1 indicates that there exist favourable groundwater conditions for further enrichment of fluoride minerals in the study area. This finding certainly shall be detrimental to the human health risks, especially of infants and children, in the long run, which is a matter of great concern for the entire study area. Chemometric modelling confirms that Ca^{2+}, Mg^{2+}, HCO_3^-, F⁻ and SO_4^{2-} are derived from geogenic sources, Cl^- and NO_3^- from anthropogenic inputs and Na^+ and K^+ from mixed factors. Further, integration of extracted principal components (PCs) with each significant cluster enables prediction of the latent parameters influencing the sampling locations and confirmation of the various sources.

The study area needs clean drinking water free from NO_3^- and F⁻ for better human health. Based on the unique findings of the present work, socio-enviro conditions and hydrogeological setup, treatment of groundwater through various membrane techniques (reverse osmosis and electrodialysis), ion exchange, adsorption, coagulation, and precipitation processes are highly recommended prior to human consumption. Also, since literacy rate in the area is about 50%, effort needs to be made for mass awareness through various IEC (information, education, and communication) techniques to apprise people of the local groundwater conditions and what is best for their longevity. Further, to tackle similar problems elsewhere in the world, the evaluation of HHRA must be carried out both deterministically and probabilistically to get a holistic picture of groundwater vulnerability. Source apportionment of the contaminants too must be conducted with the help of the chemometric techniques for better human judgement.

Data availability

The datasets generated during and/or analysed during the current study are already presented in the form of tables and figures in the manuscript. In case of any specific requirement, the corresponding author may please be contacted for the needful.

References

1. Guo, Y., Li, P., He, X. & Wang, L. Groundwater quality in and around a landfill in Northwest China: Characteristic pollutant identification, health risk assessment, and controlling factor analysis. *Expo. Health* **14**, 885–901. https://doi.org/10.1007/s12403-022-00464-6 (2022).
2. He, S., Li, P., Su, F., Wang, D. & Ren, X. Identification and apportionment of shallow groundwater nitrate pollution in Weining Plain, northwest China, using hydrochemical indices, nitrate stable isotopes, and the new Bayesian stable isotope mixing model (MixSIAR). *Environ. Pollut.* **298**, 118852. https://doi.org/10.1016/j.envpol.2022.118852 (2022).
3. Gugulothu, S., Subba Rao, N., Das, R., Duvva, L. K. & Dhakate, R. Judging the sources of inferior groundwater quality and health risk problems through intake of groundwater nitrate and fluoride from a rural part of Telangana, India. *Environ. Sci. Pollut. Res.* **29**, 49070–49091. https://doi.org/10.1007/s11356-022-18967-9 (2022).
4. Rajkumar, H., Naik, P. K., Singh, G. & Rishi, M. Hydrogeochemical characterization, multi-exposure deterministic and probabilistic health hazard evaluation in groundwater in parts of Northern India. *Toxin Rev.* **42**(1), 204–227. https://doi.org/10.1080/15569543.2022.2080222 (2023).
5. Sankara, L. & Pratap, R. S. Health risk assessment of nitrate and fluoride toxicity in groundwater contamination in the Nagarkurnool watershed region of Telangana state. *J. Appl. Geochem.* **25**(1), 9–25 (2023).
6. Arabgol, R., Sartaj, M. & Asghari, K. Predicting nitrate concentration and its spatial distribution in groundwater resources using support vector machines (SVMs) model. *Environ. Model. Assess.* **21**, 71–82. https://doi.org/10.1007/s10666-015-9468-0 (2016).
7. Zhai, Y. *et al.* Does the groundwater nitrate pollution in China pose a risk to human health? A critical review of published data. *Environ. Sci. Pollut. Res.* **24**, 3640–3653. https://doi.org/10.1007/s11356-016-8088-9 (2017).
8. Kumar, D. *et al.* Source characterization and human health risk assessment of nitrate in groundwater of middle Gangetic Plain, India. *Arab. J. Geosci.* **12**, 339. https://doi.org/10.1007/s12517-019-4519-5 (2019).
9. Wang, S. *et al.* Relationship between land-use and sources and fate of nitrate in groundwater in a typical recharge area of the North China plain. *Sci. Total. Environ.* **609**, 607–620. https://doi.org/10.1016/j.scitotenv.2017.07.176 (2017).
10. Lapworth, D. J., Krishan, G., MacDonald, A. M. & Rao, M. S. Groundwater quality in the alluvial aquifer system of Northwest India: New evidence of the extent of anthropogenic and geogenic contamination. *Sci. Total. Environ.* **599**, 1433–1444. https://doi.org/10.1016/j.scitotenv.2017.04.223 (2017).
11. Herojeet, R. K., Madhuri, S. R., Renu, L. & Ranjna, G. Application of environmetrics statistical models and water quality index for groundwater quality characterization of alluvial aquifer of Nalagarh Valley, Himachal Pradesh, India. *Sustain. Water. Resour. Manag.* **2**, 39–53. https://doi.org/10.1007/s40899-015-0039-y (2016).
12. Subba Rao, N., Dinakar, A. & Kumari, B. K. Appraisal of vulnerable zones of non-cancer-causing health risks associated with exposure of nitrate and fluoride in groundwater from a rural part of India. *Environ. Res.* **202**, 111674. https://doi.org/10.1016/j.envres.2021.111674 (2021).
13. Das, R., Subba Rao, N., Sahoo, H. K. & Sakram, G. Nitrate contamination in groundwater and its health implications in a semi-urban region of Titrol block, Jagatsinghpur district, Odisha, India. *Phys. Chem. Earth Parts A/B/C* **132**, 103424. https://doi.org/10.1016/j.pce.2023.103424 (2023).
14. Holloway, J. M. & Dahlgren, R. A. Nitrogen in rock: Occurrences and biogeochemical implications. *Global. Biogeochem. Cycles* **16**(4), 1118. https://doi.org/10.1029/2002GB001862 (2002).
15. Holloway, J. M. & Smith, R. L. Nitrogen and carbon flow from rock to water: Regulation through soil biogeochemical processes, Mokelumne River watershed, California, and Grand Valley, Colorado. *J. Geophys. Res.* **110**, F01010. https://doi.org/10.1029/2004JF000124 (2005).
16. Chica-Olmo, M. *et al.* methodology for assessing public health risk associated with groundwater nitrate contamination: A case study in an agricultural setting (southern Spain). *Environ. Geochem. Health* **39**(5), 1117–1132. https://doi.org/10.1007/s10653-016-9880-7 (2017).
17. Adimalla, N. Spatial distribution, exposure, and potential health risk assessment from nitrate in drinking water from semi-arid region of South India. *Hum. Ecol. Risk. Assess. Int. J.* **26**(2), 310–334. https://doi.org/10.1080/10807039.2018.1508329 (2020).
18. Li, P., He, X. & Guo, W. Spatial groundwater quality and potential health risks due to nitrate ingestion through drinking water: A case study in Yan'an City on the Loess Plateau of northwest China. *Hum. Ecol. Risk. Assess. Int. J.* **25**(1–2), 11–31. https://doi.org/10.1080/10807039.2018.1553612 (2019).
19. Ceballos, E., Dubny, S., Othax, N., Zabala, M. E. & Peluso, F. Assessment of human health risk of chromium and nitrate pollution in groundwater and soil of the Matanza-Riachuelo River basin, Argentina. *Expo. Health* **10**(3), 323–336. https://doi.org/10.1007/s12403-021-00386-9 (2021).
20. Feng, W., Wang, C., Lei, X., Wang, H. & Zhang, X. Distribution of nitrate content in groundwater and evaluation of potential health risks: A case study of rural areas in northern China. *Int. J. Environ. Res. Publ. Health.* **17**, 9390. https://doi.org/10.3390/ijerph17249390 (2020).
21. Carrey, R. *et al.* Combining multi-isotopic and molecular source tracking methods to identify nitrate pollution sources in surface and groundwater. *Water Res.* **188**, 116537. https://doi.org/10.1016/j.watres.2020.116537 (2021).
22. Rahmati, O., Samani, A. N., Nariman, M. & Mahdavi, M. Assessment of the contribution of N-fertilizers to nitrate pollution of groundwater in western Iran (case study: Ghorveh-Dehgelan aquifer). *Water. Qual. Expo. Health* **7**, 143–151. https://doi.org/10.1007/s12403-014-0135-5 (2015).
23. Karunanidhi, D., Aravinthasamy, P., Subramani, T., Wu, J. & Srinivasamoorthy, K. Potential health risk assessment for fluoride and nitrate contamination in hard rock aquifers of Shanmuganadhi River basin, South India. *Hum. Ecol. Risk. Assess. Int. J.* **25**(1–2), 250–270. https://doi.org/10.1080/10807039.2019.1568859 (2019).
24. Singh, G., Rishi, M. S., Herojeet, R., Kaur, L. & Sharma, K. Evaluation of groundwater quality and human health risks from fluoride and nitrate in semi-arid region of northern India. *Environ. Geochem. Health.* **42**, 1833–1862. https://doi.org/10.1007/s10653-019-00449-6 (2020).
25. Kaur, L., Rishi, M. S. & Siddiqui, A. U. Deterministic and probabilistic health risk assessment techniques to evaluate non-carcinogenic human health risk (NHHR) due to fluoride and nitrate in groundwater of Panipat, Haryana, India. *Environ. Pollut.* **259**, 113711. https://doi.org/10.1016/j.envpol.2019.113711 (2020).
26. Marghade, D., Malpe, D. B., Duraisamy, K., Patil, P. D. & Li, P. Hydrogeochemical evaluation, suitability, and health risk assessment of groundwater in the watershed of Godavari basin, Maharashtra, Central India. *Environ. Sci. Pollut. Res.* **28**, 18471–18494. https://doi.org/10.1007/s11356-020-10032-7 (2021).
27. Karunanidhi, D., Aravinthasamy, P., Subramani, T. & Kumar, M. Human health risks associated with multipath exposure of groundwater nitrate and environmentally friendly actions for quality improvement and sustainable management: A case study from Texvalley (Tiruppur region) of India. *Chemosphere* **265**, 129083. https://doi.org/10.1016/j.chemosphere.2020.129083 (2021).
28. Rai, S. N. Groundwater pollution in India—An overview. In *Groundwater Pollution. Mumbai* 419–436. (Allied Publications Pvt. Ltd., 2003).

29. Sangwan, P., Rishi, M. S. & Singh, G. Assessment of drinking water quality and non-carcinogenic health risk associated with the feed and treated water of water treatment devices (WTDs) in southwest Punjab, India. *Toxin Rev.* **41**(2), 536–550. https://doi.org/10.1080/15569543.2021.1906707 (2021).
30. Sadeq, M. *et al.* Drinking water nitrate and prevalence of methemoglobinemia among infants and children aged 1–7 years in Moroccan areas. *Int. J. Hyg. Environ. Health* **211**, 546–554. https://doi.org/10.1016/j.ijheh.2007.09.009 (2008).
31. Almasri, M. N. Nitrate contamination of groundwater: A conceptual management framework. *Environ. Impact Assess. Rev.* **27**, 220–242. https://doi.org/10.1016/j.eiar.2006.11.002 (2007).
32. Gao, Y., Yu, G., Luo, C. & Zhou, P. Groundwater nitrogen pollution and assessment of its health risks: A case study of a typical village in rural-urban continuum, China. *PLoS One* **7**(4), e33982. https://doi.org/10.1371/journal.pone.0033982 (2012).
33. Fabro, A. Y. R., Ávila, J. G. P., Alberich, M. V. E., Sansores, S. A. C. & Camargo-Valero, M. A. Spatial distribution of nitrate health risk associated with groundwater use as drinking water in Merida, Mexico. *Appl. Geogr.* **6**, 49–57. https://doi.org/10.1016/j.apgeog.2015.10.004 (2015).
34. Chang, C. C., Tsai, S. S., Wu, T. N. & Yang, C. Y. Nitrates in municipal drinking water and non-Hodgkin lymphoma: An ecological cancer case-control study in Taiwan. *J. Toxic Environ. Health A* **73**, 330–338. https://doi.org/10.1080/15287390903421243 (2009).
35. Elisante, E. & Muzuka, A. N. N. Occurrence of nitrate in Tanzanian groundwater aquifers: A review. *Appl. Water Sci.* **7**(1), 71–87. https://doi.org/10.1007/s13201-015-0269-z (2017).
36. Kumar, M., Das, A., Das, N., Goswami, R. & Singh, U. K. Co-occurrence perspective of arsenic and fluoride in the groundwater of Diphu, Assam, Northeastern India. *Chemosphere* **150**, 227–238. https://doi.org/10.1016/j.chemosphere.2016.02.019 (2016).
37. Li, P. *et al.* Occurrence and hydrogeochemistry of fluoride in shallow alluvial aquifer of Weihe River, China. *Environ. Earth Sci.* **71**(7), 3133–3145. https://doi.org/10.1007/s12665-013-2691-6 (2014).
38. Subba Rao, N., Ravindra, B. & Wu, J. Geochemical and health risk evaluation of fluoride rich groundwater in Sattenapalle Region, Guntur district, Andhra Pradesh, India. *Hum. Ecol. Risk. Assess. Int. J.* **26**(9), 2316–2348. https://doi.org/10.1080/10807039.2020.1741338 (2020).
39. Gyanendra, Y. & Alam, W. Geospatial assessment and hydrogeochemical characterization of groundwater resources of Manipur Valley, India. *Environ. Monit. Assess.* **195**, 1037. https://doi.org/10.1007/s10661-023-11584-0 (2023).
40. Sharma, D. A., Rishi, M. S. & Keesari, T. Evaluation of groundwater quality and suitability for irrigation and drinking purposes in southwest Punjab, India using hydrochemical approach. *Appl. Water Sci.* **7**(6), 3137–3150. https://doi.org/10.1007/s13201-016-0456-6 (2017).
41. Li, P., He, X., Li, Y. & Xiang, G. Occurrence and health implication of fluoride in groundwater of loess aquifer in the Chinese loess plateau: A case study of Tongchuan, Northwest China. *Expo. Health* **11**, 95–107. https://doi.org/10.1007/s12403-018-0278-x (2019).
42. Duggal, V., Goyal, T., Kaur, R., Kaur, J. & Bajaj, G. Assessment of fluoride exposure and associated health risks from different sources of drinking water to various age groups in Bathinda City, Punjab, India. *Phys. Chem. Earth Parts A/B/C* **132**, 103472. https://doi.org/10.1016/j.pce.2023.103472 (2023).
43. Adimalla, N., Li, P. & Venkatayogi, S. Hydrogeochemical evaluation of groundwater quality for drinking and irrigation purposes and integrated interpretation with water quality index studies. *Environ. Process.* **5**, 363–383. https://doi.org/10.1007/s40710-018-0297-4 (2018).
44. WHO (World Health Organization). *Guidelines for Drinking-Water Quality* 4th edn. (World Health Organization, 2011).
45. WHO (World Health Organization). *Guidelines for Drinking Water Quality Incorporating the First Addendum* 4th edn, 1–631 (World Health Organization, 2017).
46. BIS (Bureau of Indian Standards). *Indian Standard Drinking Water Specification*, 2nd ed. IS:10500 1–18. (Indian Standard Institute, 2012).
47. USPHS (United States Public Health Service). Report on fluoride benefits and risks: Review of fluoride benefits and risks. Report of the Ad Hoc Subcommittee on Fluoride (1991).
48. Wu, J., Li, P. & Qian, H. Hydrochemical characterization of drinking groundwater with special reference to fluoride in an arid area of China and the control of aquifer leakage on its concentrations. *Environ. Earth Sci.* **73**(12), 8575–8588. https://doi.org/10.1007/s12665-015-4018-2 (2015).
49. Ayoob, S. & Gupta, A. K. Fluoride in drinking water: A review on the status and stress effects. *Crit. Rev. Environ. Sci. Technol.* **36**, 433–487. https://doi.org/10.1080/10643380600678112 (2006).
50. CGWB (Central Groundwater Board). *Groundwater Quality Scenario in India* (Central Groundwater Board, Government of India, 2015).
51. Katya, C., Caroline, D., Susan, A. & Ashok, J. G. Factors governing the performance of bauxite in fluoride remediation of groundwater. *Environ. Sci. Technol.* **51**(4), 2321–2328. https://doi.org/10.1021/acs.est.6b04601 (2017).
52. Verma, A., Shetty, B. K., Guddattu, V., Chourasia, M. K. & Pundir, P. High prevalence of dental fluorosis among adolescents is a growing concern: A school based cross-sectional study from Southern India. *Environ. Health Prev. Med.* **22**, 17. https://doi.org/10.1186/s12199-017-0624-9 (2017).
53. Mukherjee, I. & Singh, U. K. Groundwater fluoride contamination, probable release, and containment mechanisms: A review on Indian context. *Environ. Geochem. Health* **40**, 2259–2301. https://doi.org/10.1007/s10653-018-0096-x (2018).
54. Chowdhary, P. *et al.* CKD of unknown origin in Supebeda, Chhattisgarh, India. *Kidney Int. Rep.* **6**(1), 210–214. https://doi.org/10.1016/j.ekir.2020.10.007 (2020).
55. John, O. *et al.* Chronic kidney disease of unknown etiology in India: What do we know and where we need to go. *Kidney Int. Rep.* **6**(11), 2743–2751. https://doi.org/10.1016/j.ekir.2021.07.031 (2021).
56. Rathore, V., Pal, R., Galhotra, A., Nayak, S., Snehalata, & Jha, V., & Nagarkar, N. M. Community perception of chronic kidney disease in Supebeda, Chhattisgarh. *IJCRR*. **14**(2):23–28. https://doi.org/10.31782/IJCRR.2022.14210 (2022).
57. CGWB (Central Groundwater Board). Groundwater quality in Supebeda area of Gariabandh district Chhattisgarh. (Central Groundwater Board, North Central Chhattisgarh Region Raipur, Department of Water resources, River Development and Ganga Rejuvenation, Ministry of Jal Shakti, Government of India, 2021).
58. Gupta, S., Bhattacharya, A., Raith, M. & Nanda, J. K. Contrasting pressure–temperature–deformation history across a vestigial craton–mobile belt boundary: The western margin of the Eastern Ghats Belt at Deobhog, India. *J. Metamorph. Geol.* **18**(6), 683–697 (2000).
59. Neogi, S. & Das, N. Lithotectonic domains and metamorphic history of the boundary zone of the Eastern Ghats mobile belt and the Bastar craton, Deobhog area, Central India. *Geol. Surv. India Spec. Publ.* **57**, 180–204 (2000).
60. Hounslow, A. *Water Quality Data: Analysis and Interpretation* (CRC Press, 2018).
61. Li, D. *et al.* Bioaccumulation and human health risk assessment of trace metals in the freshwater mussel *Cristaria plicata* in Dongting Lake, China. *J. Environ. Sci.* **104**, 335–350. https://doi.org/10.1016/j.jes.2020.12.012 (2021).
62. USEPA (U.S. Environmental Protection Agency). *Guidelines for Exposure Assessment. Federal Register Notice 57*, 22887–22938. (Risk Assessment Forum, U.S. Environmental Protection Agency, 1992).
63. Ma, Y., Egodawatta, P., McGree, J., Liu, A. & Goonetilleke, A. Human health risk assessment of heavy metals in urban stormwater. *Sci. Total Environ.* **557–558**, 764–772. https://doi.org/10.1016/j.scitotenv.2016.03.067 (2016).

64. USEPA (U.S. Environmental Protection Agency). Exposure factors handbook ed (Final), http://cfpub.epa.gov/ncea/risk/recordisplay.cfm?deidD236252. (US Environmental Protection Agency, 2011).
65. Rodriguez-Proteau, R. & Grant, R. L. Toxicity evaluation and human health risk assessment of surface and groundwater contaminated by recycled hazardous waste materials. *Handb. Environ. Chem. 5 Part F* **2**, 133–189 (2005).
66. Saha, N. *et al.* Industrial metal pollution in water and probabilistic assessment of human health risk. *J. Environ. Manag.* **185**, 70–78. https://doi.org/10.1016/j.jenvman.2016.10.023 (2017).
67. USEPA (U.S. Environmental Protection Agency). *Risk Assessment Guidance for Superfund Volume I: Human Health Evaluation Manual (Part E, Supplemental Guidance for Dermal Risk Assessment).* (US Environment Protection Agency, 2004).
68. USEPA (U.S. Environmental Protection Agency). *A Review of the Reference Dose and Reference Concentration Processes* 1–192. U.S. Environmental Protection Agency, Risk Assessment Forum, EPA/630/P-02/002F (2002).
69. USEPA (U.S. Environmental Protection Agency). *Integrated Risk Information System.* https://cfpub.epa.gov/ncea/iris/search/index.cfm. (United States Environmental Protection Agency, 2012).
70. Ali, S. *et al.* Health risk assessment due to fluoride exposure from groundwater in rural areas of Agra, India: Monte Carlo simulation. *Int. J. Environ. Sci. Technol.* **18**, 3665–3676. https://doi.org/10.1007/s13762-020-03084-2 (2021).
71. Lin, M. L., Gui, H. R. & Peng, W. H. Health risk assessment of heavy metals in the groundwater of a coal mining area in northern Anhui province, China. *Nat. Environ. Pollut. Technol.* **15**, 11–18 (2016).
72. USEPA (U.S. Environmental Protection Agency). *Guiding Principles for Monte Carlo Analysis. Risk Assessment Forum* 1–23. (U.S. Environmental Protection Agency, 1997).
73. Jamal, A. *et al.* Distribution and health risk assessment of heavy metals in soil surrounding a lead and zinc smelting plant in Zanjan. *Iran. Hum. Ecol. Risk. Assess. Int. J.* **25**(4), 1018–1033. https://doi.org/10.1080/10807039.2018.1460191 (2019).
74. Ganyaglo, S. Y. *et al.* Groundwater fluoride contamination and probabilistic health risk assessment in fluoride endemic areas of the Upper East Region, Ghana. *Chemosphere* **233**, 862–872. https://doi.org/10.1016/j.chemosphere.2019.05.276 (2019).
75. Singh, G., Rishi, M. S., Herojeet, R., Kaur, L. & Sharma, K. Multivariate analysis and geochemical signatures of groundwater in the agricultural dominated taluks of Jalandhar district, Punjab, India. *J. Geochem. Explor.* **208**, 106395. https://doi.org/10.1016/j.gexplo.2019.106395 (2020).
76. Herojeet, R., Rishi, M. S. & Kishore, N. Integrated approach of heavy metal pollution indices and complexity quantification using chemometric models in the Sirsa Basin, Nalagarh valley, Himachal Pradesh, India. *Chin. J. Geochem.* **34**, 620–633. https://doi.org/10.1007/s11631-015-0075-1 (2015).
77. Sharma, G. *et al.* Application of multivariate statistical analysis and water quality index for quality characterization of Parbati River, Northwestern Himalaya, India. *Discov. Water* **1**, 5. https://doi.org/10.1007/s43832-021-00005-3 (2021).
78. Nayak, A., Matta, G. & Uniyal, D. P. Hydrochemical characterization of groundwater quality using chemometric analysis and water quality indices in the foothills of Himalayas. *Environ. Dev. Sustain.* https://doi.org/10.1007/s10668-022-02661-4 (2022).
79. Herojeet, R., Rishi, M. S., Lata, R. & Konchok, D. Quality characterization and pollution source identification of surface water using multivariate statistical techniques, Nalagarh Valley, Himachal Pradesh, India. *Appl. Water Sci.* **7**(5), 2137–2156. https://doi.org/10.1007/s13201-017-0600-y (2017).
80. Simeonov, V., Simeonova, P. & Tsitouridou, R. Chemometric quality assessment of surface waters: Two case studies. *Chem. Eng. Ecol.* **11**(6), 449–469 (2004).
81. Khalid, S. An assessment of groundwater quality for irrigation and drinking purposes around brick kilns in three districts of Balochistan province, Pakistan, through water quality index and multivariate statistical approaches. *J. Geochem. Explor.* **197**, 14–26. https://doi.org/10.1016/j.gexplo.2018.11.007 (2019).
82. Rajkumar, H., Naik, P. K. & Rishi, M. S. Evaluation of heavy metal contamination in soil using geochemical indexing approaches and chemometric techniques. *Int. J. Environ. Sci. Technol.* **16**(11), 7467–7486. https://doi.org/10.1007/s13762-018-2081-4 (2019).
83. Kaiser, H. F. The application of electronic computers to factor analysis. *Educ. Psychol. Meas.* **20**, 141–151 (1960).
84. Shrestha, S. & Kazama, F. Assessment of surface water quality using multivariate statistical techniques: A case study of the Fuji River basin, Japan. *Environ. Model. Softw.* **22**, 464–475. https://doi.org/10.1016/j.envsoft.2006.02.001 (2007).
85. Wai, W. W., Alkarkhi, A. F. M. & Easa, A. M. Comparing biosorbent ability of modified citrus and durian rind pectin. *Carbohydr. Polym.* **79**(3), 584–589. https://doi.org/10.1016/j.carbpol.2009.09.018 (2010).
86. Rajkumar, H., Naik, P. K. & Rishi, M. S. A new indexing approach for evaluating heavy metal contamination in groundwater. *Chemosphere* **245**, 125598. https://doi.org/10.1016/j.chemosphere.2019.125598 (2020).
87. Papazova, P. & Simeonova, P. Environmetric data interpretation to assess the water quality of Maritsa River catchment. *J. Environ. Sci. Health Part A* **48**(8), 963–972. https://doi.org/10.1080/10934529.2013.762743 (2013).
88. CGWB (Central Groundwater Board) and CPCB (Central Pollution Control Board). Status of groundwater quality and pollution aspect in NCT-Delhi. In *Unpublished Report by Central Groundwater Board and Central Pollution Control Board* 1–209 (1999).
89. FAO (Food and Agriculture Organization). FAO Irrigation and Drainage Paper, 29 Rev. 1 (1994).
90. Davis, S. N. & DeWiest, R. J. *Hydrogeology* (Wiley, 1966).
91. Freeze, R. A. & Cherry, J. A. *Groundwater* (Prentice-Hall, 1979).
92. Sawyer, G. N. & McCarthy, D. L. *Chemistry of Sanitary Engineers* 2nd edn, 518 (McGraw Hill, 1967).
93. Sidhu, N., Rishi, M. S. & Herojeet, R. K. Groundwater quality variation with respect to aquifer dispositioning in urbanized watershed of Chandigarh, India. *Int. J. Env. Ecol. Fam. Urban Stud.* **3**(2), 87–98 (2013).
94. Carlsson, S., Wiklund, N. P., Engstrand, L., Weitzberg, E. & Lundberg, J. O. Effects of pH, nitrite, and ascorbic acid on nonenzymatic nitric oxide generation and bacterial growth in urine. *Nitric Oxide* **5**, 580–586 (2001).
95. Institute of Medicine, Food and Nutrition Board. *Dietary References Intakes for Calcium, Phosphorous, Magnesium, Vitamin D, and Fluoride* (National Academies Press, 1997).
96. National Research Council. *Fluoride in Drinking Water: A Scientific Review of EPA's Standards* (The National Academies Press, 2006).
97. Zhang, Y. *et al.* Implementation of long-term assessment of human health risk for metal contaminated groundwater: A coupled chemical mass balance and hydrodynamics model. *Ecotoxicol. Environ. Saf.* **180**(30), 95–105. https://doi.org/10.1016/j.ecoenv.2019.04.053 (2019).
98. Gibbs, R. J. Mechanisms controlling world water chemistry. *Science* **170**(3962), 1088–1090. https://doi.org/10.1126/science.170.3962.1088 (1970).
99. Arveti, N., Sarma, M. R. S., Aitkenhead-Peterson, J. A. & Sunil, K. Fluoride incidence in groundwater: A case study from Talupula, Andhra Pradesh, India. *Environ. Monit. Assess.* **172**, 427–443. https://doi.org/10.1007/s10661-010-1345-3 (2011).
100. Subba Rao, N. Controlling factors of fluoride in groundwater in a part of South India. *Arab. J. Geosci.* **10**, 524. https://doi.org/10.1007/s12517-017-3291-7 (2017).
101. Ma, B., Jin, M., Liang, X. & Li, J. Groundwater mixing and mineralization processes in a mountain–oasis–desert basin, northwest China: Hydrogeochemistry and environmental tracer indicators. *Hydrogeol. J.* **26**(1), 233–250. https://doi.org/10.1007/s10040-017-1659-0 (2018).
102. Adimalla, N. & Wu, J. Groundwater quality and associated health risks in a semi-arid region of south India: Implication to sustainable groundwater management. *Hum. Ecol. Risk. Assess.* **25**(1–2), 191–216. https://doi.org/10.1080/10807039.2018.1546550 (2019).

103. Aravinthasamy, P., Karunanidhi, D., Subramani, T., Srinivasamoorthy, K. & Anand, B. Geochemical evaluation of fluoride contamination in groundwater from Shanmuganadhi River basin, South India: Implication on human health. *Environ. Geochem. Health* **42**, 1937–1963. https://doi.org/10.1007/s10653-019-00452-x (2020).

104. Herojeet, R. K., Rishi, S. M. & Sidhu, N. Hydrochemical characterization, classification and evaluation of groundwater regime in Sirsa watershed, Nalagarh Valley, Himachal Pradesh, India. *Civ. Environ. Res.* **3**(7), 47–57 (2013).

105. Lata, R., Rishi, M. S., Dolma, K., Herojeet, R. & Kaur, L. Major ion chemistry and water quality index for surface water quality characterization in parts of Kinnaur District, Himachal Pradesh, India. *Environ. Ecol.* **39**(1), 109–128 (2021).

106. Nematollahi, M. J., Clark, M. J. R., Ebrahimi, P. & Ebrahimi, M. Preliminary assessment of groundwater hydrogeochemistry within Gilan, a northern province of Iran. *Environ. Monit. Assess.* **190**(4), 242. https://doi.org/10.1007/s10661-018-6543-4 (2018).

107. Kolsi, S. H., Bouri, S., Hachicha, W. & Ben, D. H. Implementation and evaluation of multivariate analysis for groundwater hydrochemistry assessment in arid environments: A case study of Hajeb ElyounJelma, Central Tunisia. *Environ. Earth Sci.* **70**, 2215–2224. https://doi.org/10.1007/s12665-013-2377-0 (2013).

108. Yadav, S., Bansal, S. K., Yadav, S. & Kumar, S. Fluoride distribution in undergroundwater of district Mahendergarh, Haryana, India. *Appl. Water. Sci.* **9**, 1–11. https://doi.org/10.1007/s13201-019-0935-7 (2019).

109. Adams, S., Titus, R., Pietersen, K., Tredoux, G. & Harris, C. Hydrochemical characteristics of aquifers near Sutherland in the Western Karoo, South Africa. *J. Hydrol.* **241**, 91–103. https://doi.org/10.1016/S0022-1694(00)00370-X (2001).

110. Adimalla, N. & Venkatayogi, S. Mechanism of fluoride enrichment in groundwater of hard rock aquifers in Medak, Telangana State, South India. *Environ. Earth. Sci.* **76**, 45. https://doi.org/10.1007/s12665-016-6362-2 (2017).

111. Subba Rao, N. High-fluoride groundwater. *Environ. Monit. Assess.* **176**, 637–645. https://doi.org/10.1007/s10661-010-1609-y (2011).

112. Bahir, M., Ouazar, D. & Ouhamdouch, S. Characterization of mechanisms and processes controlling groundwater salinization in coastal semi-arid area using hydrochemical and isotopic investigations (Essaouira basin, Morocco). *Environ. Sci. Pollut. Res.* **25**, 24992–25004. https://doi.org/10.1007/s11356-018-2543-8 (2018).

113. Adimalla, N. & Venkatayogi, S. Geochemical characterization and evaluation of groundwater suitability for domestic and agricultural utility in semi-arid region of Basara, Telangana State, South India. *Appl. Water. Sci.* **8**, 44. https://doi.org/10.1007/s13201-018-0682-1 (2018).

114. Reddy, B. A., Sunithaa, V., Prasad, M., Reddy, Y. S. & Reddy, M. R. Evaluation of groundwater suitability for domestic and agricultural utility in semi-arid region of Anantapur, Andhra Pradesh State, South India. *Groundw. Sustain. Dev.* **9**, 100262. https://doi.org/10.1016/j.gsd.2019.100262 (2019).

115. Dadgar, P. & Payandeh, P. E. Investigation of nitrate concentration and its correlation with water pH in drinking water distribution network of the City of Tabriz. *Int. J. Sci. Stud.* **5**(4), 726–731. https://doi.org/10.17354/ijssI/2017/98 (2017).

116. Keesari, T. *et al.* High fluoride in groundwater of an industrialized area of Eastern India (Odisha): Inferences from geochemical and isotopic investigation. *Environ. Earth. Sci.* **75**, 1090. https://doi.org/10.1007/s12665-016-5874-0 (2016).

117. Raju, A. & Singh, A. Assessment of groundwater quality and mapping human health risk in central Ganga Alluvial Plain, Northern India. *Environ. Process.* **4**, 375–397. https://doi.org/10.1007/s40710-017-0232-0 (2017).

118. Karunanidhi, D. *et al.* Evaluation of non-carcinogenic risks due to fluoride and nitrate contaminations in a groundwater of an urban part (Coimbatore region) of south India. *Environ. Monit. Assess.* **192**, 102. https://doi.org/10.1007/s10661-019-8059-y (2020).

119. Paul, R., Brindha, K., Gowrisankar, G., Tan, M. L. & Singh, M. K. Identification of hydrogeochemical processes controlling groundwater quality in Tripura, Northeast India using evaluation indices, GIS, and multivariate statistical methods. *Environ. Earth. Sci.* **78**(15), 470. https://doi.org/10.1007/s12665-019-8479-6 (2019).

120. Gimenez, E. Caracterizacion hidrogeoquimica de los procesos de salinizacion del aquifero detritico cotero de la Plana de Castellon. Ph. D. thesis, Universidad de Granada (1994).

121. Jalali, M. Nitrate pollution of groundwater in Toyserkan, western Iran. *Environ. Earth Sci.* **62**, 907–913. https://doi.org/10.1007/s12665-010-0576-5 (2011).

122. Zhou, Y., Li, P., Xue, L., Dong, Z. & Li, D. Solute geochemistry and groundwater quality for drinking and irrigation purposes: A case study in Xinle City, North China. *Geochemistry* **80**(4), 125609. https://doi.org/10.1016/j.chemer.2020.125609 (2020).

123. Keesari, T. *et al.* Isotope and hydrochemical systematics of groundwater from multi-tiered aquifer in central parts of Indo-Gangetic Plains, India—Implications on groundwater sustainability and security. *Sci. Total Environ.* **789**, 147860. https://doi.org/10.1016/j.scitotenv.2021.147860 (2021).

124. Zhang, Q., Xu, P. & Qian, H. Groundwater quality assessment using improved water quality index (WQI) and human health risk (HHR) evaluation in a semi-arid region of Northwest China. *Expo. Health* **12**, 487–500. https://doi.org/10.1007/s12403-020-00345-w (2020).

125. Das, B. K. & Kaur, P. Major ion chemistry of Renuka lake and weathering processes, Sirmaur district, Himachal Pradesh, India. *Environ. Geol.* **40**(7), 908–917. https://doi.org/10.1007/s002540100268 (2001).

126. Subramani, T., Rajmohan, N. & Elango, L. Groundwater geochemistry and identification 538 of hydrogeochemical processes in a hard rock region, Southern India. *Environ. Monit. Assess.* **162**(1–4), 123–137. https://doi.org/10.1007/s10661-009-0781-4. 540 (2010).

127. Mahaqi, A., Moheghi, M. M., Mehiqi, M. & Moheghy, M. A. Hydrogeochemical characteristics and groundwater quality assessment for drinking and irrigation purposes in the Mazar-i-Sharif city North Afghanistan. *Appl. Water Sci.* **8**, 133. https://doi.org/10.1007/s13201-018-0768-9 (2018).

128. Rajmohan, N. & Elango, L. Identification and evolution of hydrogeochemical processes in the groundwater environment in an area of the Palar and Cheyyar River Basins, Southern India. *Environ. Geol.* **46**, 47–61. https://doi.org/10.1007/s00254-004-1012-5 (2004).

129. Adimalla, N. Groundwater quality for drinking and irrigation purposes and potential health risks assessment: A case study from semi-arid region of South India. *Expo. Health* **11**, 109–123. https://doi.org/10.1007/s12403-018-0288-8 (2019).

130. McQuillan, D. Ground-water quality impacts from on-site septic systems. In *Proceedings, National Onsite Wastewater Recycling Association, 13th Annual Conference* 6–18 (2004).

131. Sajil Kumar, P. J., Jegathambal, P. & James, E. J. Chemometric evaluation of nitrate contamination in the groundwater of a hard rock area in Dharapuram, South India. *Appl. Water Sci.* **4**(4), 397–405. https://doi.org/10.1007/s13201-014-0155-0 (2014).

132. Suthar, S. *et al.* Nitrate contamination in groundwater of some rural areas of Rajasthan, India. *J. Hazard. Mater.* **171**(1–3), 189–199. https://doi.org/10.1016/j.jhazmat.2009.05.111 (2009).

133. Subba Rao, N. Groundwater quality from a part of Prakasam District, Andhra Pradesh, India. *Appl. Water Sci.* **8**, 30. https://doi.org/10.1007/s13201-018-0665-2 (2018).

134. Narsimha, A. & Sudarshan, V. Hydrogeochemistry of groundwater in Basara area, Adilabad district, Andhra Pradesh, India. *J. Appl. Geochem.* **15**(2), 224–237 (2013).

135. Purushothaman, P. *et al.* Evaluation of hydrogeochemistry and water quality in Bist-Doab region, Punjab, India. *Environ. Earth Sci.* **72**(3), 693–706. https://doi.org/10.1007/s12665-013-2992-9 (2014).

136. Kumari, R., Datta, P. S., Rao, M. S., Mukherjee, S. & Azad, C. Anthropogenic perturbations induced groundwater vulnerability to pollution in the industrial Faridabad District, Haryana India. *Environ. Earth. Sci.* **77**, 187. https://doi.org/10.1007/s12665-018-7368-8 (2018).

137. Van Breemen, N. Soil forming processes in acid sulfate soils. 66–130. In *Acid Sulfate Soils. Proceedings of International Symposium* (ed Dost, H.), 1st edn. 13–20 (1973).

138. Arya, S., Subramani, T., Vennila, G. & Karunanidhi, D. Health risks associated with fluoride intake from rural drinking water supply and inverse mass balance modelling to decipher hydrogeochemical processes in Vattamalaikarai River basin, South India. *Environ. Geochem. Health* **43**, 705–716. https://doi.org/10.1007/s10653-019-00489-y (2019).

139. Handa, B. K. Geochemistry and genesis of fluoride containing groundwaters in India. *Groundwater* **13**, 275–281. https://doi.org/10.1111/j.1745-6584.1975.tb03086.x (1975).

140. Salve, P. R., Maurya, A., Kumbhare, P. S., Ramteke, D. S. & Wate, S. R. Assessment of groundwater quality with respect to fluoride. *Bull. Environ. Contam. Toxicol.* **81**, 289–293. https://doi.org/10.1007/s00128-008-9466-x (2008).

141. Xiao, Y. *et al.* Occurrence, controlling factors and health hazards of fluoride-enriched groundwater in the lower flood plain of Yellow River, Northern China. *Expo. Health* **14**, 345–358. https://doi.org/10.1007/s12403-021-00452-2 (2022).

142. Karunanidhi, D., Aravinthasamy, P., Deepali, M., Subramani, T. & Shankar, K. Groundwater pollution and human health risks in an industrialized region of Southern India: Impacts of the COVID-19 lockdown and the monsoon seasonal cycles. *Arch. Environ. Contam. Toxicol.* **80**, 259–276. https://doi.org/10.1007/s00244-020-00797-w (2021).

143. Saxena, V. K. & Ahmed, S. Inferring the chemical parameters for the dissolution of fluoride in groundwater. *Environ. Geol.* **143**, 731–736. https://doi.org/10.1007/s00254-002-0672-2 (2003).

144. Jacks, G., Bhattacharya, P., Chaudhary, V. & Singh, K. P. Controls on the genesis of some high fluoride groundwaters in India. *Appl. Geochem.* **20**, 221–228. https://doi.org/10.1016/j.apgeochem.2004.07.002 (2005).

145. Hem, J. D. Study and interpretation of the chemical characteristics of natural water, Jodhpur, India, 3rd edn, 97. United States Geological Survey Professional Paper 2254. (Scientific Publications, 1991).

146. Karthikeyan, K., Nanthakumar, K., Velmurugan, P., Tamilarasi, S. & Lakshmanaperumalsamy, P. Prevalence of certain inorganic constituents in groundwater samples of Erode district, Tamil Nadu, India, with special emphasis on fluoride, fluorosis and its remedial measures. *Environ. Monit. Assess.* **160**, 141–155. https://doi.org/10.1007/s10661-008-0664-0 (2010).

147. Tirumalesh, K., Shivanna, K. & Jalihal, A. A. Isotope hydrochemical approach to understand fluoride release into groundwaters of Ilkal area, Bagalkot district, Karnataka, India. *Hydrogeol. J.* **15**, 589–598. https://doi.org/10.1007/s10040-006-0107-3 (2007).

148. Panwar, M., Jha, M. P., Khandelwal, D. & Khandelwal, K. Hydro-geochemical study of high fluoride in groundwater with help of GIS application: A case study of Kishangarh, district Ajmer, Rajasthan. In *Frontiers of Earth Science* (eds Shrivastava, K. L. & Shrivastava, P. K.) 297–304 (Scientific Publishers, 2015).

149. Dey, R. K. *et al.* Hydrogeochemical processes controlling the high fluoride concentration in groundwater: A case study at the Boden block area, Orissa, India. *Environ. Monit. Assess.* **184**, 3279–3291. https://doi.org/10.1007/s10661-011-2188-2 (2012).

150. Maitra, A., Keesari, T., Roy, A. & Gupta, S. Fluoride contamination in and around selected geothermal sites in Odisha, Eastern India: Assessment of ionic relations, fluoride exposure and remediation. *Environ. Sci. Pollut. Res.* **28**, 18553–21856. https://doi.org/10.1007/s11356-020-10948-0 (2021).

151. Keesari, T. *et al.* High fluoride in groundwater of an industrialized area of Eastern India (Odisha): Inferences from geochemical and isotopic investigation. *Environ. Earth Sci.* **75**, 1090. https://doi.org/10.1007/s12665-016-5874-0 (2016).

152. Dinka, M. O., Loiskandlb, W. & Ndambukic, J. M. Hydrochemical characterization of various surface water and groundwater resources available in Matahara areas, Fantalle Woreda of Oromiya region. *J. Hydrol. Reg. Stud.* **3**, 444–456. https://doi.org/10.1016/j.ejrh.2015.02.007 (2015).

153. Krishnaraj, S. *et al.* Use of hydrochemistry and stable isotopes as tools for groundwater evolution and contamination investigations. *Geoscience* **1**(1), 16–25. https://doi.org/10.5923/j.geo.20110101.02 (2011).

154. Kim, S. H., Kim, K., Ko, K. S., Kim, Y. & Lee, K. S. Co-contamination of arsenic and fluoride in the groundwater of unconsolidated aquifers under reducing environments. *Chemosphere* **87**(8), 8510–8856. https://doi.org/10.1016/j.chemosphere.2012.01.025 (2012).

155. Raj, D. & Shaji, E. Fluoride contamination in groundwater resources of Alleppey, southern India. *Geosci. Front.* **8**(1), 117–124. https://doi.org/10.1016/j.gsf.2016.01.002 (2017).

156. Amadi, P. A., Ofoegbu, C. O. & Morrison, T. Hydrogeochemical assessment of groundwater quality in parts of the Niger Delta, Nigeria. *Environ. Geol. Water Sci.* **14**, 195–202. https://doi.org/10.1007/BF01705131 (1987).

157. Okiongbo, K. S. & Douglas, R. K. Evaluation of major factors influencing the geochemistry of groundwater using graphical and multivariate statistical methods in Yenagoa city, Southern Nigeria. *Appl. Water Sci.* **5**, 27–37. https://doi.org/10.1007/s13201-014-0166-x (2015).

Author contributions

H.R.: Conceptualization, software, formal analysis, data curation, methodology, writing—original draft preparation. R.K.D.: Field investigations, water sampling and chemical analysis. P.K.N.: Visualization, supervision, validation, writing—reviewing and editing. J.R.V.: Hydrogeological investigations, water sampling and preparation of maps. All authors have read and approved the final manuscript. The authors affirm that human research participants provided informed consent for publication of the images in Graphical Abstract. In case of minors, informed consent was obtained from all subjects and/or their legal guardian(s).

Competing interests

The authors declare no competing interests.

Additional information

Supplementary Information The online version contains supplementary material available at https://doi.org/10.1038/s41598-023-45622-1.

Correspondence and requests for materials should be addressed to P.K.N.

Reprints and permissions information is available at www.nature.com/reprints.

Publisher's note Springer Nature remains neutral with regard to jurisdictional claims in published maps and institutional affiliations.